JOC Article

A Strategy for the Synthesis of Metal Bis(2,2′:6′,2″-terpyridine)-Terminated Molecular Dyads Having Controlled Torsion Angles at the Central Biphenyl Linker

Andrew C. Benniston,* Anthony Harriman, Peiyi Li, Pritesh V. Patel, and Craig A. Sams

Molecular Photonics Laboratory, School of Natural Sciences, Bedson Building, University of Newcastle, Newcastle upon Tyne NE1 7RU, United Kingdom

a.c.benniston@ncl.ac.uk

Received January 10, 2006

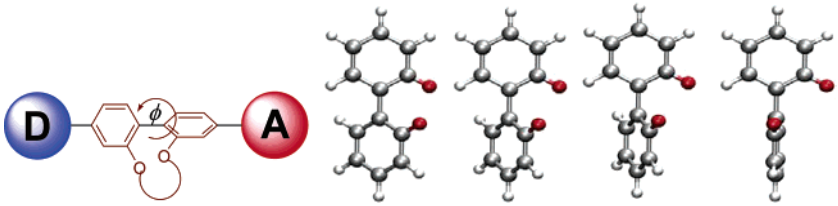

The synthesis of a series of binuclear complexes comprising bis(2,2′:6′,2″-terpyridine)ruthenium(II) and -osmium(II) centers connected via a geometrically constrained 4,4′-biphenyl bridge is described. These compounds have been prepared by a "synthesis-at-metal" approach as well as by the conventional method of synthesizing the ligand and subsequently attaching the metal center. A computational investigation into the behavior of the biphenyl-based bridges has been used to provide lowest-energy conformations and to estimate the degree of internal fluctuation about the mean torsion angle. It is shown that the length of the constraining strap determines both the torsion angle and the internal flexibility, with longer straps twisting the biphenyl group so as to relax stereochemical interactions between the linking oxygen atoms. Longer straps can be formed from poly(ethylene glycol) residues that provide an additional binding site for small cations. Electrospray mass spectrometry carried out on solutions of these crown ether-like bridges confirmed that Li^+, Na^+, and K^+ ions bind in the form of 1:1 complexes. This range of compounds should permit rational examination of how the torsion angle affects the rate of through-bond electron transfer, electron exchange, and charge shift.

Introduction

Among the many goals of contemporary molecular chemistry are the design and synthesis of artificial photosynthetic units and molecular photonic devices.[1] The operation of such systems relies heavily on through-bond electron-transfer processes, and an important design element involves the capacity to control the rate of light-induced and thermal electron flow.[2] A potential methodology by which to accomplish this formidable task is to build a variable rotor into the framework that connects the terminals and that modulates the central torsion angle so as to tune the rate of electron transfer.[3] This approach has several attractions, including the possibility to switch the conformation by exposure to short laser pulses, and ultimately will result in the availability of one central unit for use in all prototypic examples. An added bonus would arise if the rates of charge separation and charge recombination could be discriminated by way of bridge topology.[4] Progress in the field has been slow, most notably because of the severe difficulty associated with

* To whom correspondence should be addressed. Tel: + 44 (0)191 222 5706. Fax: + 44 (0)191 222 8660.

(1) (a) Garcia-Parajo, M. F.; Hernando, J.; Mosteiro, G. S.; Hoogenboom, J. P.; van Dijk, E. M. H. P.; van Hulst, N. F. *ChemPhysChem* **2005**, *6*, 819. (b) Tinnefeld, P.; Heilemann, M.; Sauer, M. *ChemPhysChem* **2005**, *6*, 217. (c) Heilemann, M.; Tinnefeld, P.; Sanchez Mosteiro, G.; Garcia Parajo, M.; Van Hulst, N. F.; Sauer, M. *J. Am. Chem. Soc.* **2004**, *126*, 6514. (d) Hindin, E.; Forties, R. A.; Loewe, R. S.; Ambroise, A.; Kirmaier, C.; Bocian, D. F.; Lindsey, J. S.; Holten, D.; Knox, R. S. *J. Phys. Chem. B* **2004**, *108*, 12821. (e) Terazono, Y.; Kodis, G.; Andreasson, J.; Jeong, G. J.; Brune, A.; Hartmann, T.; Durr, H.; Moore, A. L.; Morre, T. A.; Gust, D. *J. Phys. Chem. B* **2004**, *108*, 1812. (f) Ambroise, A.; Kirmaier, C.; Wagner, R. W.; Loewe, R. S.; Bocian, D. F.; Holten, D.; Lindsey, J. S. *J. Org. Chem.* **2002**, *67*, 3811. (g) Wagner, R. W.; Lindsey, J. S. *J. Am. Chem. Soc.* **1994**, *116*, 9759. (h) Weiss, E. A.; Ahrens, M. J.; Sinks, L. E.; Gusev, A. V.; Ratner, M. A.; Wasielewski, M. R. *J. Am. Chem. Soc.* **2004**, *126*, 5577. (i) Stadler, R.; Forshaw, M.; Joachim, C. *Nanotechnology* **2003**, *14*, 138. (j) Robertson, N.; McGowan, C. A. *Chem. Soc. Rev.* **2003**, *32*, 96. (k) Benniston, A. C. *Chem. Soc. Rev.* **2004**, *33*, 573. (l) Holten, D.; Bocian, D. F.; Lindsey, J. S. *Acc. Chem. Res.* **2002**, *35*, 57.

10.1021/jo0600555 CCC: $33.50
Published on Web 04/05/2006

the design of suitable molecular prototypes where the geometry of the connector can be varied systematically over a wide range.[5] To isolate the effects of bridge topology on the dynamics of electron transfer, it is crucial that the electronic properties of the bridge are kept constant. This is a daunting challenge!

We now describe a generic solution to this problem, based on the synthesis of tethered biphenyl-based linkers.[6] The tether is connected through alkoxy groups at the 2,2′-positions such that the electronic properties are unaffected by the composition of the tether. The latter can be elongated in small increments, and heteroatoms or ring structures can be incorporated at predetermined sites. The advantages of including heteroatoms into the tether include improved solubility and the capacity to bind adventitious species from solution.[7] The length of the tether, and the nature of any bound substrates, helps to control the torsion angle at the center of the biphenyl group.[8] Because electron transfer along aromatic units, such as polyphenylenes,[9] is markedly more effective than along hydrocarbon chains,[10] electron flow will proceed through the biphenyl linker regardless of torsion angle. This allows the first rational examination of how the rate of electron transfer depends on torsion angle. The nature of the terminals is irrelevant, provided they facilitate injection and capture of electronic energy. Here, we use transition metal bis(2,2′:6′,2″-terpyridine) complexes as light- and redox-active terminals, but these could easily be replaced with specific units.

The synthesis, purification, and characterization of these molecules is far from easy. Potential pitfalls include the isolation of atropisomers and the lack of structural integrity because of internal rotation.[11] The latter problem can be overcome by immobilization of the molecular unit in a solid support, such as a frozen glass. An additional problem relates to the precise determination of the central torsion angle under operating conditions. It is also important to consider ways whereby electron transfer might bypass the angle dependence. This could include nuclear tunneling and/or vibrational coupling.[12] Such properties cannot be evaluated without access to suitable molecules, however, and so the first step is the synthesis of a set of appropriate molecules that will fully confront the general "angle dependence" concept.

An intriguing possibility then follows: how to switch the conformation quickly and reversibly between optimum limits. This would provide for unidirectional electron transfer and could lead to the identification of unusually long-lived, charge-separated states. Research into conformational gating is ongoing but is hindered by the scarcity of knowledge regarding the optimum geometries for fast electron transfer.[13] It might be that different types of electron-transfer processes, for example, charge separation, charge recombination, and charge shift, display markedly disparate angle dependencies. This would open the door to the future development of novel optoelectronic devices. Here, we describe our research into the synthesis of geometrically constrained bridges. A later paper will report on the rate of electron exchange in these molecules under varying experimental conditions, although preliminary results obtained in a glassy matrix have been reported and firmly establish that the dynamics of electron flow depend precisely on the central torsion angle.[14]

Results and Discussion

The main objective of this research is to isolate a set of compounds that will permit examination of how the rate of through-bond electron transfer depends on the torsion angle of a bridging biphenyl unit. Such information, which is not currently available, is required for the design of next-generation optoelectronic devices, for the optimization of artificial photosynthetic units, and for an improved understanding of biological electron transfer. Because the rates of different types of electron-transfer processes might exhibit disparate angle dependencies, a universal approach was sought. That is to say, the maximum number of independent studies need to be made from the same set of compounds. To that end, we opted to synthesize molecular dyads possessing metal (M = Ru^{II} or Os^{II}) bis(2,2′:6′,2″-terpyridine) complexes as the light- and redox-active terminals. The mixed-metal $Ru^{II}-Os^{II}$ complexes are ideal candidates for the detailed study of electron exchange between the terminals;[15] this process corresponds to simultaneous hole and electron transfer.[16] Selective oxidation of the Os^{II} terminal, giving rise to the mixed-metal, mixed-valence $Ru^{II}-Os^{III}$ complexes, facilitates the study of light-induced electron transfer across the same connector. Partial oxidation of the binuclear Ru^{II} complexes forms the mixed-valence $Ru^{II}-Ru^{III}$ complexes which display intervalence charge-transfer absorption bands in the near-IR region.[17] This permits exploration of the angle dependence for hole transfer. The binuclear Ru^{II} complexes are weakly luminescent[18] and can be exploited to study how the torsion angle influences the extent of electron delocalization at the triplet level.[19] Oxidation to the corresponding binuclear Ru^{III} complexes introduces ligand-to-metal, charge-transfer absorption bands in the far-red region.[20] Although cationic terminals restrict solubility in nonpolar solvents, the wide versatility in redox chemistry makes these complexes suitable targets for our investigations.

(2) (a) Goldsmith, R. H.; Sinks, L. E.; Kelley, R. F.; Betzen, L. J.; Liu, W.; Weiss, E. A.; Ratner, M. A.; Wasielewski, M. R. *Proc. Natl. Acad. Sci. U.S.A.* **2005**, *102*, 3540. (b) Skourtis, S.; Nitzan, A. *J. Chem. Phys.* **2003**, *119*, 6271. (c) Weiss, E. A.; Ahrens, M. J.; Sinks, L. E.; Gusev, A. V.; Ratner, M. A.; Wasielewski, M. R. *J. Am. Chem. Soc.* **2004**, *126*, 5577. (d) Hayes, R. T.; Wasielewski, M. R.; Gosztola, D. *J. Am. Chem. Soc.* **2000**, *122*, 5563.

(3) (a) Helms, A.; Heiler, D.; McLendon, G. *J. Am. Chem. Soc.* **1991**, *113*, 4325. (b) Maus, M.; Rettig, W.; Bonafoux, D.; Lapouyade, R. *J. Phys. Chem. A* **1999**, *103*, 3388.

(4) (a) Rubtsov, I. V.; Redmore, N. P.; Hochstrasser, R. M.; Therien, M. J. *J. Am. Chem. Soc.* **2004**, *126*, 2684. (b) Fukuzumi, S.; Kotani, H.; Ohkubo, K.; Ogo, S.; Tkachenko, N. V.; Lemmetyinen, H. *J. Am. Chem. Soc.* **2004**, *126*, 1600. (c) Benniston, A. C.; Harriman, A.; Li, P.; Rostron, J. P.; van Ramesdonk, H. J.; Groeneveld, M. M.; Zhang, H.; Verhoeven, J. W. *J. Am. Chem. Soc.* **2005**, *127*, 16054.

(5) (a) Seth, J.; Palaniappan, V.; Wagner, R. W.; Johnson, T. E.; Lindsey, J. S.; Bocian, D. F. *J. Am. Chem. Soc.* **1996**, *118*, 11194. (b) Osuka, A.; Maruyama, K.; Mataga, N.; Asahi, T.; Yamazaki, I.; Tamai, N. *J. Am. Chem. Soc.* **1990**, *112*, 4958. (c) Benniston, A. C.; Harriman, A.; Li, P.; Sams, C. A.; Ward, M. D. *J. Am. Chem. Soc.* **2004**, *126*, 13630.

(6) Benniston, A. C.; Harriman, A.; Li, P.; Sams, C. A. *Tetrahedron Lett.* **2003**, *44*, 4167.

(7) Benniston, A. C.; Li, P.; Sams, C. A. *Tetrahedron Lett.* **2003**, *44*, 3947.

(8) Benniston, A. C.; Harriman, A.; Patel, P. V.; Sams, C. A. *Eur. J. Org. Chem.* **2005**, 4680.

(9) (a) Beckers, E. H. A.; Meskers, S. C. J.; Schenning, A. P. H.; Chen, F. W.; Janssen, R. A. J. *J. Phys. Chem. A* **2004**, *108*, 6933. (b) Ramos, A. M.; Beckers, E. H. A.; Offermans, T.; Meskers, S. C. J.; Janssen, R. A. *J. Phys. Chem. A.* **2004**, *108*, 8201.

(10) Paulson, B. P.; Curtiss, L. A.; Bal, B.; Closs, G. L.; Miller, J. R. *J. Am. Chem. Soc.* **1996**, *118*, 378.

(11) Wolf, C.; Konig, W. A.; Roussel, C. *Liebigs. Ann. Chem.* **1995**, 781.

(12) Ohkita, H.; Benten, H.; Anada, A.; Noguchi, H.; Kido, N.; Ito, S.; Yamamoto, M. *Phys. Chem. Chem. Phys.* **2004**, *6*, 3977.

(13) Weiss, E. A.; Tauber, M. J.; Kelley, R. F.; Ahrens, M. J.; Ratner, M. A.; Wasielewski, M. R. *J. Am. Chem. Soc.* **2005**, *127*, 11842.

(14) Benniston, A. C.; Harriman, A.; Li, P.; Patel, P. V.; Sams, C. A. *Phys. Chem. Chem. Phys.* **2005**, *7*, 3677.

It is well-known that most ruthenium(II) bis(2,2′:6′,2″-terpyridine) complexes are nonluminescent at room temperature,[21] unlike the corresponding tris(2,2′-bipyridine) complexes.[22] However, these latter complexes are chiral and thereby introduce unnecessary problems for characterization. Emission can be enhanced significantly by attaching an alkyne at the 4′-position of the terpyridine ligand; this approach causes a significant prolongation of the triplet lifetime.[23] Thus, the compounds studied here are equipped with suitable alkynylene substituents. Because the Os^{II} fragment can be excited selectively at long wavelength,[24] it is not necessary to isolate the binuclear Os^{II} complexes. The binuclear Ru^{II} complexes are needed, however, as reference compounds.

A second, and equally important aim, is to establish the geometry of the bridging connector under operating conditions. Our approach to this problem involves the combined use of molecular mechanics and molecular dynamics simulations. The former work addresses the lowest-energy conformation while the latter relates to internal flexibility. Related work[25] has demonstrated that simpler derivatives of the biphenyl-based connector having additional oxygen atoms built into the tether bind cations from solution.[8] The affinity toward particular cations depends on the length of the tethering strap. It was also shown that the bound cation affects the central torsion angle, as might be expected from the rigidification that occurs on filling the central void.[26]

Compound Abbreviations. To simplify identification for each compound, a generic abbreviation scheme is used and is explained as follows: The abbreviations **R** and **O** correspond to the 2,2′:6′,2″-terpyridine fragments containing the cations ruthenium(II) and osmium(II), respectively. The ditopic 2,2′:6′,2″-terpyridine ligands containing one to four methylene units are numbered **C1**−**C4**, respectively, whereas the crown ether containing ligands are represented by **CE4**−**CE6**, where the number indicates the number of oxygen atoms in the ring. Thus, bimetallic homonuclear complexes contain **R** before and after the ligand abbreviation, whereas heteronuclear complexes contain **R** and **O** at the beginning and end. The compounds comprising the isolated biphenyl unit from the bridging ligand but lacking the metallo-terminals are designated as **BP**, followed by the corresponding abbreviation for the type of constraining strap.

Synthesis. The most widespread method for preparation of binuclear transition metal complexes is to first synthesize the ditopic ligand before attaching a single metal center at one end.[27] This generally works well for creation of homoleptic complexes[28] but can be problematic when mixed-metal complexes are required. It has been long recognized that multitopic ligands based on 2,2′:6′,2″-terpyridine (terpy) generally suffer from poor solubility.[29] Ziessel and co-workers[30] have circumvented this problem by the attachment of long alkyl chains to the bridge segment of their ditopic ligands. However, this method is not always possible, and as a consequence, the "synthesis-at-metal" approach is gaining in popularity.[31] Outlined in Scheme 1 are the synthetic methods employed here; it highlights the use of both classical and metal synthon approaches. The linked derivatives **1a**−**g** were prepared by mild deprotonation of 4,4′-diiodobiphenyl-2,2′-diol and subsequent reaction with the readily prepared (or commercially available) diiodoalkyl or ditosyloxy-polyether linkers. The yields of the final products varied from 36% for **1g** to 65% for **1b**. The cross-coupling of **1a**−**d**,**f** with 4-ethynyl-2,2′:6′,2″-terpyridine[71] using standard Sonogashira coupling conditions[32] afforded the alkoxy-strapped ligands **C1**−**C4** and **CE5**, respectively. Ligand **C1** is particularly insoluble in common organic solvents, which aided its purification since all impurities were simply washed from the crude reaction mixture to leave the target compound. On the other hand, ligands **C2**−**C4** and **CE5** are readily soluble in common organic solvents and were purified by column chromatography. Refluxing either **C2**−**C3** or **CE5** in an acetone/methanol/chloroform (2:1:1) mixture with 2 equiv of **3** afforded, after column chromatography, complexes **RC2R**, **RC3R**, and **RCE5R** in 40−60% yield. Attempts to prepare the monoruthenium(II) synthons **RCn** (n = 2, 3) and **RCE5** met with limited success. In all cases, the amount of material obtained was insufficient to prepare the corresponding mixed-metal Ru^{II}−Os^{II} complexes; instead, the dinuclear complexes were isolated as the major products.

To prepare the mixed-metal complexes, the alternative route of carefully coupling **1** to the synthon **4** was used, again under standard Sonogashira conditions.[32] Typically, an acetonitrile solution of **4** was added over a period of 24 h to a refluxing solution of **1a**−**g** in THF/CH_3CN (3:1) containing $Pd(PPh_3)_2Cl_2$, CuI, and $^iPr_2NH$. Careful column chromatographic separation (silica gel) of the crude reaction mixture afforded the monoiodo derivatives **5a**−**g** in modest yields (20−42%). Despite using a 1:1 stoichiometry of **4** to **1a**−**g**, the coupling reactions

(15) Barigelletti, F.; Flamigni, L.; Collin, J.-P.; Sauvage, J.-P. *Chem. Commun.* **1997**, 333.
(16) El-ghayoury, A.; Harriman, A.; Ziessel, R. *J. Phys. Chem. A* **2000**, *104*, 7906.
(17) Launay, J.-P. *Chem. Soc. Rev.* **2001**, *30*, 386.
(18) Harriman, A.; Khatyr, A.; Ziessel, R.; Benniston, A. C. *Angew. Chem., Int. Ed.* **2000**, *39*, 4287.
(19) Benniston, A. C.; Harriman, A.; Li, P.; Sams, C. A. *Phys. Chem. Chem. Phys.* **2004**, *6*, 875.
(20) (a) Naklicki, M. L.; Crutchley, R. J. *J. Am. Chem. Soc.* **1994**, *116*, 6045. (b) Evans, C. E. B.; Yap, G. P. A.; Crutchley, R. J. *Inorg. Chem.* **1998**, *37*, 6161.
(21) Winkler, J. R.; Netzel, T. L.; Creutz, C.; Sutin, N. *J. Am. Chem. Soc.* **1987**, *109*, 2381.
(22) Caspar, J. V.; Meyer, T. J. *J. Am. Chem. Soc.* **1983**, *105*, 5583.
(23) Benniston, A. C.; Grosshenny, V.; Harriman, A.; Ziessel, R. *Angew. Chem., Int. Ed. Engl.* **1994**, *33*, 1884.
(24) Krausz, E.; Riesen, H. *Coord. Chem. Rev.* **1997**, *159*, 9.
(25) Bhattacharyya, S.; Sousa, L. R.; Ghosh, S. *Chem. Phys. Lett.* **1997**, *269*, 314.
(26) Varnek, A.; Wipff, G. *J. Mol. Struct.* **1996**, *363*, 67.
(27) (a) Constable, E. C.; Figgemeier, E.; Housecroft, C. E.; Olsson, J.; Zimmermann, Y. C. *Dalton Trans.* **2004**, 1918. (b) Barbieri, A.; Ventura, B.; Barigelletti, F.; De Nicola, A.; Quesada, M.; Ziessel, R. *Inorg. Chem.* **2004**, *43*, 7359. (c) Akasaka, T.; Inoue, H.; Kuwabara, M.; Mutai, T.; Otsuki, J.; Araki, K. *Dalton Trans.* **2003**, 815. (d) Harriman, A.; Hissler, M.; Khatyr, A.; Ziessel, R. *Chem Commun.* **1999**, 735. (e) Borgström, M.; Johansson, O.; Lomoth, R.; Berglund Baudin, H.; Wallin, S.; Sun, L.; Åkermark, B.; Hammarström, L. *Inorg. Chem.* **2003**, *42*, 5173. (f) Chiorboli, C.; Rodgers, M. A. J.; Scandola, F. *J. Am. Chem. Soc.* **2003**, *125*, 483. (g) Akasaka, T.; Mutai, T.; Oysuki, J.; Araki, K. *Dalton Trans.* **2003**, 1537. (h) Steenwinkel, P.; Grove, D. M.; Veldman, N.; Spek, A. L.; von Koten, G. *Organometallics* **1998**, *17*, 5655.
(28) Cargill Thompson, A. M. W. *Coord. Chem. Rev.* **1997**, *160*, 1.
(29) Grosshenny, V.; Romero, F. M.; Ziessel, R. *J. Org. Chem.* **1997**, *62*, 1491.
(30) Khatyr, A.; Ziessel, R. *J. Org. Chem.* **2000**, *65*, 3126.
(31) (a) Fraysse, S.; Coudret, C.; Launay, J.-P. *J. Am. Chem. Soc.* **2003**, *125*, 5880. (b) Benniston, A. C.; Mitchell, S.; Rostron, S. A.; Yang, S. *Tetrahedron Lett.* **2004**, *45*, 7883. (c) Ziessel, R.; Grosshenny, V.; Hissler, M.; Stroh, C. *Inorg. Chem.* **2004**, *43*, 4262. (d) Welter, S.; Salluce, N.; Benetti, A.; Rot, N.; Belser, P.; Sonar, P.; Grimsdale, A. C.; Müllen, K.; Lutz, M.; Spek, A. L.; De Cola, L. *Inorg. Chem.* **2005**, *44*, 4706.
(32) Sonogashira, K.; Tohda, Y.; Hagihara, N. *Tetrahedron Lett.* **1975**, *50*, 4467.

SCHEME 1[a]

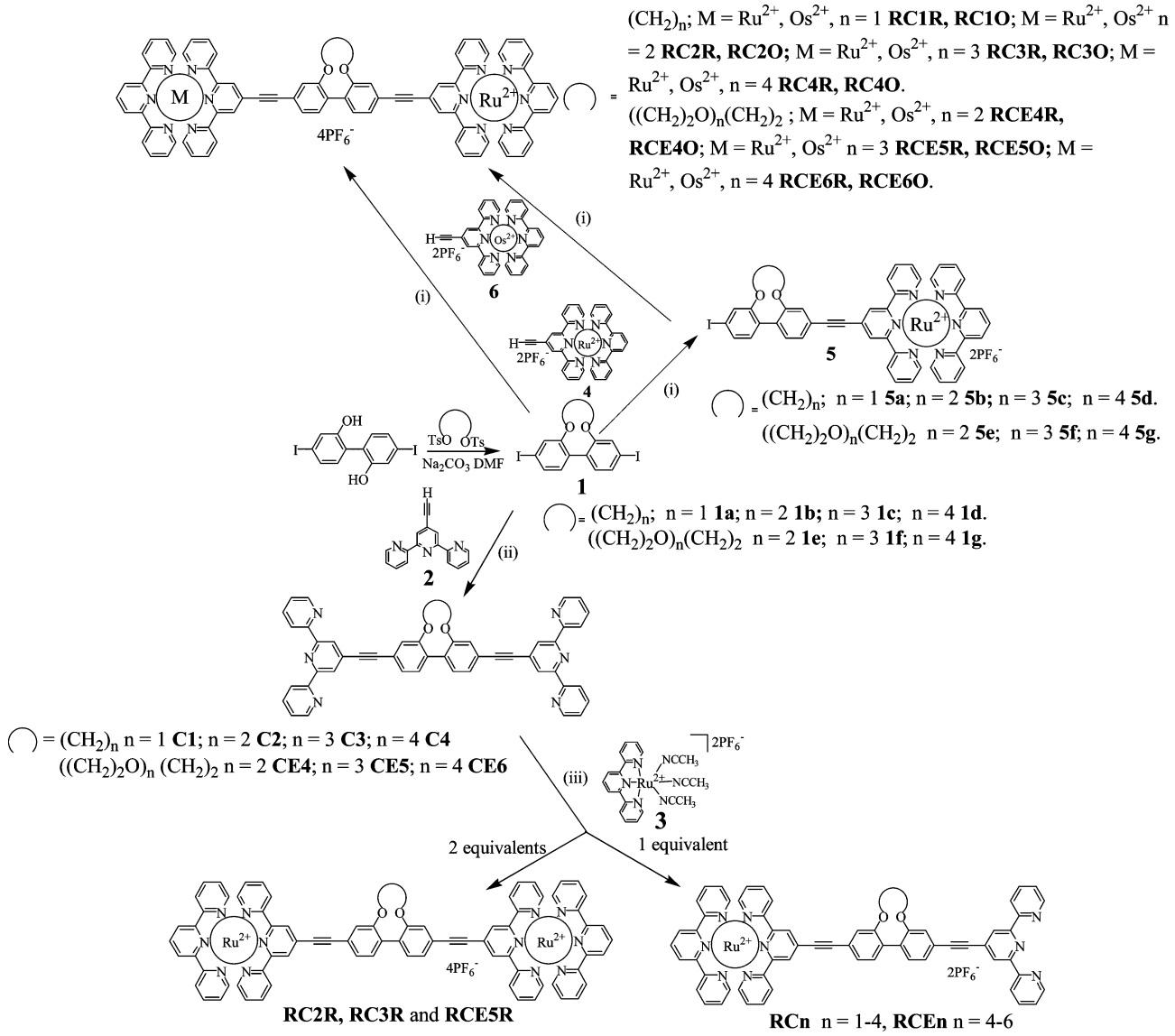

[a] Reagents and conditions: (i) $Pd(PPh_3)_2Cl_2$, CuI, $^iPr_2NH$, THF/CH_3CN, reflux, 48 h; (ii) $Pd(PPh_3)_2Cl_2$, CuI, $^iPr_2NH$, THF, reflux, 48 h, (iii) acetone, methanol, chloroform (2:1:1), reflux, 24 h.

always produced significant quantities of the binuclear complexes **RCnR** ($n = 1-4$) and **RCEnR** ($n = 4-6$). Because of the relative ease of this method, preparation of the homobinuclear complexes was carried out as highlighted above but with 2 equiv of **4**. Cross-coupling of **5a**−**g** with the osmium-containing synthon **6** yielded the hetero-binuclear complexes **RCnO** ($n = 1-4$) and **RCEnO** ($n = 4-6$) in varying yields (23−42%). The low yields reflect, to some degree, the difficulty in purification of the final products, which involved repeated column chromatography. A further advantage of producing synthons **5a**−**g** is their capacity to be used as precursors for much larger linear arrays, through cross coupling to a $[M(terpy-\equiv-H)_2]^{2+}$ (M = Os(II), Ru(II), Zn(II), etc.) central core.[33]

Identification and check on purity for the various metal complexes relied on the use of ^1H NMR spectroscopy, electrospray (ES) and MALDI mass spectrometry, and elemental analysis. The characteristic ^1H NMR shifts for the alkyl and alkoxy signals of the bridge units are easily identified in the spectra for these complexes. Also, the singlet resonances at ca. 8.9 ppm and triplet resonances at ca. 8.4 ppm corresponding to the 3′, 5′, and 4′ protons of the substituted and unsubstituted terpyridine ligands, respectively, easily confirmed attachment of the Ru-terpy and Os-terpy units. The ES and MALDI mass spectral records for the complexes displayed a cluster of peaks corresponding to cations identified as $[M - nPF_6]^{m+}$ fragments, with theoretical and observed isotopic patterns in excellent agreement.

Variable Temperature ^1H NMR Spectroscopy. Internal rotation of the biphenyl unit is hindered in ligands **C1**−**C4** and **CE4**−**CE6** which can, in principle, lead to the isolation of atropisomers. Previously published molecular modeling studies performed on **C3** in vacuo identified two isomers created by restricted C−C bond rotation.[6] In view of this finding, similar behavior was expected for the other ligands. Close inspection of the ^1H NMR region associated with the alkoxy groups for

(33) Benniston, A. C.; Harriman, A.; Li, P.; Sams, C. A. *J. Am. Chem. Soc.* **2005**, *127*, 2553.

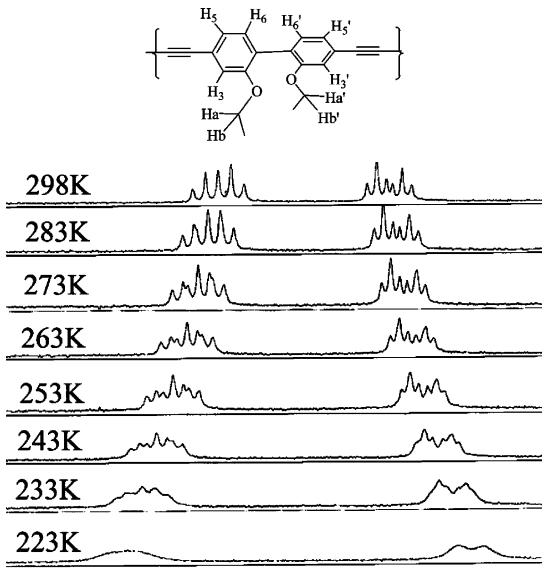

FIGURE 1. Partial 500 MHz ^{1}H NMR spectrum between 4.1 and 4.5 ppm for **RCE5R** in CD_3CN**,** showing the methylene signals associated with the bridging unit. Note that the Ru-terpy portion and the remainder of the alkoxy strap have been omitted from the figure for clarity.

the free ligands and metal complexes confirmed that the bridge undergoes hindered rotation. As an example, variable-temperature ^{1}H NMR spectra were obtained for **RCE5R** in CD_3CN to gain further insight into these fluxional processes. Illustrated in Figure 1 is a typical set of proton resonances for the OCH_2 signals associated with the bridging biphenyl group. At ambient temperature, two clear signals are observed at 4.4 and 4.2 ppm which each correspond to a doublet of triplets. On cooling the solution, the most downfield signals alter in appearance and shift to higher frequency, whereas the other signals shift upfield and broaden. The two distinct alterations in chemical shifts suggest that the environment of the protons has changed upon cooling. Signals associated exclusively with the biphenyl unit also undergo substantial shifts (see the Supporting Information). In particular, the doublets at 7.45 and 7.44 ppm corresponding to H_3,$H_{3'}$ and H_5,$H_{5'}$, respectively, are shifted downfield and broadened to such an extent that at 253 K the signals could not be discerned from the baseline. This observed temperature dependence for the NMR signals is associated with slowing of the twisting of the biphenyl unit, coupled with a reduction in rocking of the OCH_2 unit. That in solution the two atropisomers readily interconvert is consistent with previous studies into biphenyl-based systems.[34] Generally, isolation of the two isomeric forms is achieved by "locking up" rotation around the aryl−aryl bond by metal ion binding[35] or by synthetic means.[36] It is worth noting that these NMR studies also confirm that, at very low temperature (77 K), the outlined motions will be essentially frozen, such that the variation in dihedral torsion angle will be minimal.[14]

Binding Studies for 1e−g Toward Alkali Cations. The compounds **CE4**−**CE6** are expected to bind cations (e.g., Li^+, Na^+, K^+) in the void provided by the crown ether macrocycle. Since ligands **CE4**−**CE6** contain, in principle, three cation binding sites (two terpy ligands and one crown ether) and to simplify matters, binding studies were performed on the precursors **1e**−**g**. In preliminary work, it was found that ^{1}H NMR spectroscopy was too insensitive to identify, by chemical shifts, cation binding in these precursors. Likewise, ^{13}C NMR resonances were observed to shift upon addition of aliquots of metal salts, but data were too imprecise to afford rational binding constants. Unequivocal evidence for cation binding was obtained instead from electrospray (ES) mass spectrometry, in particular, with acetonitrile/water mixtures containing equimolar concentration of Li^+, Na^+, and K^+ and **1e**−**g** at different stoichiometries. For each ligand, molecular ions were observed in the ES mass spectra that correspond to 1:1 metal ion/ligand adducts, with no discernible peaks that could be assigned to the 1:2 or 2:1 metal ion/ligand species (see the Supporting Information). The mass spectrum of **1e** in the presence of cations contains a single peak at $m/z = 559$ that corresponds to the Li^+ adduct. That no peaks could be observed corresponding to the Na^+ and K^+ adducts supports the selectivity of the four-oxygen containing crown ether for the small Li^+ cation.[37] In contrast, the mass spectra for **1f** in the presence of cations contained three peaks at $m/z = 603$ (63%), 619 (100%), and 635 (5%), respectively. Hence, the crown ether ligand **1f** displays selectivity for the Na^+ cation. Three peaks in the mass spectrum for the cation adducts of **1g** are located at $m/z = 647$(6%), 663 (19%), and 679 (100%). The selectivity in this case of the largest crown ether is toward the K^+ ion. It might be argued that cation binding to the binuclear metal ion complexes would be less efficient because of electrostatic repulsion, as discussed in the next section. However, it was observed that under appropriate conditions the ES mass spectra of **RCEnR** ($n = 5-6$) exhibits a cluster of peaks corresponding to the corresponding cation adducts. As an example, the ES mass spectrum of **RCE5R** (see the Supporting Information), as well as displaying a major peak at $m/z = 2003$ for the $[M - PF_6]^+$ ion, also exhibits a minor cluster of peaks ($m/z = 2187$) indicative of the KPF_6 adduct. The extraneous K^+ comes from the synthetic procedure of producing the hexafluorophosphate salt.

Although it was not possible to obtain equilibrium constants for cation/ligand binding, these results are fully supported by our previous fluorescence binding studies[8] using the nonhalogenated biphenyl analogues **BPCEn** ($n = 4-6$). Binding constants (K) measured in acetonitrile at room-temperature vary from $K = 3\ M^{-1}$ for Li^+ binding to the four oxygen crown ether, to $K = 7370\ M^{-1}$ for K^+ adduct formation with the crown-6 polycycle.[8] Hence, we are confident that cations bind to the crown ether segment of the ruthenium(II) and osmium(II) complexes; this interaction alters the conformation of the biphenyl unit and the connecting polyether chain as described below.

Molecular Modeling. Since the discovery of crown ethers by Pedersen,[38] this class of molecule has been subjected to numerous computational studies in order to ascertain ground-state conformations in the presence and absence of bound cations.[39] It is recognized that for single cyclic polyether systems such as 12-crown-4, 15-crown-5, and 18-crown-6 the molecules are able to sample a number of similar conformations along an extensive energy surface.[40] The incorporation of less flexible groups, such as phenyl and cyclohexyl, into the polyether

(34) (a) Imai, Y.; Zhang, W.; Kida, T.; Nakatsuji, Y.; Ikeda, I. *J. Org. Chem.* **2000**, *65*, 3326. (b) Mann, E.; Montero, A.; Maestro, M. A.; Herradón, B. *Helv. Chim. Acta* **2002**, *85*, 3624.

(35) Mikami, K.; Aikawa, K.; Yusa, Y.; Jodry, J. J.; Yamanaka, M. *Synlett* **2002**, 1561.

(36) Lloyd-Williams, P.; Giralt, E. *Chem. Soc. Rev.* **2001**, *30*, 145.

(37) Gafni, A.; Cohen, Y. *J. Org. Chem.* **1997**, *62*, 120.

(38) Pedersen, C. J. *J. Am. Chem. Soc.* **1967**, *89*, 7017.

backbone restricts the number of accessible conformations. In the crown ether cases presented here, and the fully alkyl chain-linked assemblies, the insertion of a biphenyl unit is expected to behave similarly.

The connecting strap linking the two phenyl rings of the molecular bridge for **C1**−**C4** and **CE4**−**CE6** is expected to control (to varying degrees) the dihedral torsion angle. Attempts were made to grow suitable crystals of all ligands and final complexes and obtain torsion angles for the biphenyl units; this met with limited success. Suitable diffraction quality crystals were obtained of **CE5**[41] and of the metal synthon **RC1**[42] incorporating a C_1 alkyl chain (see the Supporting Information). Since packing effects are known to reduce the torsion angle in biphenyl,[43] molecular modeling calculations were used to elucidate meaningful molecular structures pertinent to fluid solution and isolated molecules. Minimum energy conformations were computed using different methods (see the Experimental Section for details), but the structures obtained were all fairly similar. In each case, the geometry around the metal terminal is that of a distorted octahedron, which accounts well for the short triplet lifetimes found for the various ruthenium(II) complexes,[44] and which has been established by X-ray crystallography for many mononuclear complexes.[45] It is realized, however, that the biphenyl-based bridge is likely to be in a state of dynamic fluctuation in solution at ambient temperature[46] such that the lowest energy conformation is only one of many possible geometries for each system. Consequently, molecular dynamics simulations (MDS) were performed in order to gauge the relative flexibility of the bridging units. The target molecules **RCnR** and **RCEnR** are ca. 35 Å in length, and the metal-to-metal distance does not vary significantly throughout the MDS run. In general, there is no tendency for the substituted terpyridine ligand to adopt a coplanar arrangement with the central biphenyl unit, and instead the two units seem to maintain an almost constant dihedral angle of ca. 90° with respect to each other. This may seem surprising as there is no obvious restriction to rotation about these units but it was a generic feature of all the calculations, regardless of starting geometry.

The title compounds differ only in the nature of the bridging ligand, and it is the biphenyl-based bridging unit that shows the most notable variations in geometry as the length of the connecting tether increases.The strap undergoes dynamic fluctuation but the dihedral angle (ϕ) around the central C−C connecting bond of the biphenyl group tends toward a fixed value, regardless of starting geometry. The dihedral angles computed for the lowest-energy conformation found for **RCnR** ($n = 1-4$) are reported in Table 1. It is encouraging to note that different levels of calculation gave essentially the same result, although the overall geometry of the strap differed in each case; semiempirical methods (Gaussian-03) were applied to **BPCn** and molecular mechanics methods (Insight-II) were used for **RCnR**. It was found that, for the lowest-energy conformations ϕ increases systematically, from 37° for **RC1R** to 94° for **RC4R (**Figure 2). A similar, albeit less pronounced, effect was observed for the lowest-energy conformations computed for **RCEnR** ($n = 4-6$) where the variation in ϕ was restricted to 10°. The polyether chains are relatively expanded and they remain so during MDS runs but it is clear that a wide range of geometries is possible for the straps. It is interesting to note that as the length of the strap increases throughout the entire series of compounds the phenoxyl oxygen atoms are forced further apart.

Formation of an inclusion complex reduces ϕ by a significant amount; for example, binding Na^+ to **RCE5R** decreases the angle from 125° to 83°. The bound cation compresses the crown ether in its attempt to obtain the optimal fit around the

TABLE 1. Results Collected from Computational Studies Performed on the Constrained, Binuclear Complexes and, Where Appropriate, Their Cation Adducts

	dihedral angle (deg)			
compd	minimum energy conformation angle[a]	mean[b]	standard deviation[b]	range[b]
RC1R	37	41	6.1	± 17
RC2R	55	58	7.3	± 24
RC3R	67	70	9.4	± 30
RC4R	94	97	13.1	± 35
RCE4R	122	126	7.7	± 31
RCE4R + Li^+	60	62	8.8	± 26
RCE4R + Na^+	77	70	16.7	± 32
RCE5R	125	130	9.9	± 32
RCE5R + Li^+	61	52	10.0	± 20
RCE5R + Na^+	83	57	7.5	± 25
RCE5R + K^+	113	91	12.7	± 40
RCE6R	130	131	11.3	± 31
RCE6R + Li^+	52	51	7.6	± 27
RCE6R + Na^+	58	58	8.2	± 27
RCE6R + K^+	62	62	8.4	± 28

[a] Calculated using InsightII. [b] Calculated from Molecular Dynamics Simulations (MDS). All results are from calculations that were performed on compounds in vacuo.

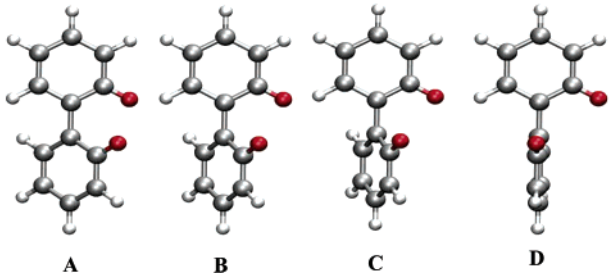

FIGURE 2. Representation of variation in the dihedral angle of the bridging unit for **RC1R** (A), **RC2R** (B), **RC3R** (C), and **RC4R** (D)**.** Note that the terminals and the connecting hydrocarbon strap have been removed for clarity.

(39) (a) El-Azhary, A. A.; Al-Kahtani, A. A. *J. Phys. Chem. A* **2005**, *109*, 8041. (b) El-Azhary, A. A.; Al-Kahtani, A. A. *J. Phys. Chem. A* **2004**, *108*, 9601. (c) Su, C. C. *J. Mol. Struct.* **2004**, *702*, 23. (d) Su, C. C.; Lu, L. H.; Liu, L. K. *J. Phys. Chem. A* **2003**, *107*, 4563. (d) Anderson, J. D.; Paulsen, E. S.; Dearden, D. V. *Int. J. Mass Spectrom.* **2003**, *227*, 63. (e) Golebiowski, J.; Lamare, V.; Ruiz-Lopez, M. F. *J. Comput. Chem.* **2002**, *23*, 724. (f) Grotjahn, M.; Lehman, S.; Aurich, J.; Holdt, H. J.; Kleinpeter, E. *J. Phys. Org. Chem.* **2001**, *14*, 43. (g) Buchanan, G. W.; Laister, R. C.; Yap, G. P. A. *J. Mol. Struct.* **2000**, *523*, 261.

(40) Al-Jallal, N. A.; El-Azhary, A. A.; Al-Kahtani, A. A. *J. Phys. Chem. A* **2005**, *109*, 3694.

(41) Benniston, A. C.; Clegg, W.; Harrington, R. W.; Li, P. *Acta Crystallogr. E* **2004**, *E60*, 02452.

(42) Although crystals were obtained for **RC1** they were extremely small and very weakly diffracting; data collected were not suitable for publication. The main features of the molecular structure, however, could be clearly identified as illustrated in the Supporting Information.

(43) Dzyabcheenko, A.; Scheraga, H. A. *Acta Crystallogr. B* **2004**, *60*, 228.

(44) Rillema, D. P.; Jones, D. S.; Woods, C.; Levy, H. A. *Inorg. Chem.* **1992**, *31*, 2935.

(45) Pyo, S.; Perez-Cordero, E.; Bott, S. G.; Echegoyne, L. *Inorg. Chem.* **1999**, *38*, 3337.

(46) Barich, D. H.; Pugmire, R. J.; Grant, D. M.; Iuliucci, R. J. *J. Phys. Chem. A* **2001**, *105*, 6780.

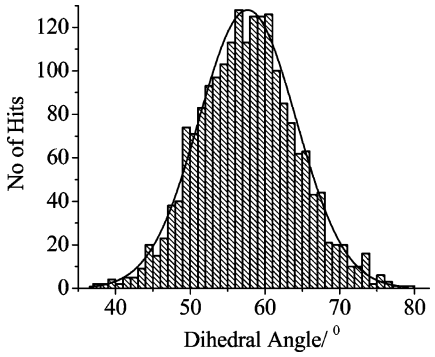

FIGURE 3. Histogram representing the variation in dihedral angle for compound **RC2R** during a MDS.

coordinating oxygen atoms and serves to rigidify the strap.[47] Interestingly, the size of the bound cation determines ϕ for **RCE5R** but in the case of **RCE6R** the dihedral angle seems to be almost independent of the nature of the cation (Table 1). It is well-known that the geometry of the inclusion complex depends on the mutual sizes of cavity and cation[48] while further geometry optimization can result from changes in solvent and or counterion.[8,49] It was noted that K^+ did not appear to form an inclusion complex with **RCE4R** and that Na^+ fits poorly into the cavity. Each cation appears to bind well to **RCE5R**, forming well-defined inclusion complexes, where increasing size of the cation forces the phenoxyl oxygen atoms further apart. In contrast, Li^+ forms a family of inclusion complexes with **RCE6R** because of its relatively small size and facile mobility among the oxygen atoms, although there is a preference for binding to the phenoxyl oxygen atoms.

These compounds are expect to reside in dynamic motion in solution[50] such that there will be considerable variation in the dihedral angle. Indeed, for the most constrained system, **RC1R**, MDS studies showed that ϕ varies by $\pm 17°$, and larger variations are found for the other systems (Table 1). For the hydrocarbon strapped systems, the variation in the dihedral angle increases with increasing strap length, as might be expected in view of the progressive increase in internal flexibility, and reaches $\pm 35°$ for **RC4R**. The MDS data can be represented in histogram form, detailing the number of times a certain angle is sampled during a simulation. As an example, the histogram calculated for **RC2R** is shown as Figure 3. Using a statistical analysis of the histogram, which corresponds to a Gaussian form, the mean, standard deviation, and angle range were derived (Table 1). These values allow a more complete description of the system and afford information on the average angle and how closely the values are collected around the mean. There is reasonably good agreement between the mean ϕ and that determined independently from the lowest energy conformation. As the length of the strap increases, both the standard deviation and the range of angles accessed increase. It should be noted that complete rotation around the connecting C−C bond is prevented by the tether. Indeed, calculations made for 2,2′-dimethoxybiphenyl, in which the dihedral angle was varied through 180° and the geometry optimized every 2°, show that as ϕ approaches 0° the biphenyl unit bends owing to repulsion between the oxygen atoms. From this calculation, the rotational energy barrier is estimated to be ca. 90 kJ mol^{-1}. This barrier is sufficient to impose atropisomerism onto the system,[51] although this was not evident from the NMR studies.

The MDS studies for **RCEnR** ($n = 4-6$) show a variation in ϕ of $\pm 32°$, which indicates the strap is not particularly effective at imposing a preferred dihedral angle at ambient temperature. These studies confirm that the inclusion complex formed with an added cation has a different ϕ value to the starting crown ether and that the bound cation rigidifies the strap. For example, binding Li^+ to **RCE5R** causes the variation of the dihedral angle to decrease from $\pm 31°$ to $\pm 20°$. This trend can be seen for each of the crown ethers (Table 1). Again, analysis of the histograms shows the mean dihedral angle to be in good agreement with that of the lowest-energy conformation and that increasing strap length leads to an increase in internal flexibility.

Evaluation of Electrostatic Effect upon Cation Binding. Previously, we reported that certain small cations bind to biphenyl-based crown ethers of direct relevance to the systems described here.[8] It is realized, however, that the full systems possess cationic terminals that might hinder the attachment of an ancillary cation because of electrostatic repulsion, although related work has shown that both 2,2′-bipyridyl[52] and 2,2′,6,6′-bipyrimidine[53] bridged, binuclear Ru-terpy complexes are able to bind added cations at the central connector. The likely importance of electrostatic repulsion on the binding free energy change can be estimated using a simple Coulomb law, taking account of the realization that the electronic charge on each ruthenium center is partially off-loaded onto the coordinated terpy ligands.[54] As a typical example, the formation of an inclusion complex between Na^+ and **RCE5R** is illustrated. The electrostatic effect was computed after first splitting the molecule into three sections; namely, the two termini and the crown ether-based connector. The partial charges for the Ru-terpy were calculated using the Discover module within Insight II and with the ESFF force field. The corresponding partial charges for the isolated biphenyl unit were calculated using a DFT method, B3LYP with a 6-31G(d) basis set, within Gaussian 03. It is recognized that this latter method is likely to be much more accurate, but too time-consuming to be applied to the complex as a whole, especially in a solvent reservoir. The partial charges were calculated for the minimum energy conformation and the electrostatic potential energy map constructed using the Poisson−Boltzmann finite difference method[55] (Figure 4). The electrostatic interaction was calculated for each pair of charges, using a linear gradient approach[56] and taking a continuum dielectric constant of 37. In Figure 4, areas of negative charge are shown in red, with the two phenoxyl atoms oriented toward to center of the cavity. The oxygen atoms in the polyether strap

(47) Wallace, W.; Chen, C.; Eyring, E. M.; Petrucci, S. *J. Phys. Chem.* **1985**, *89*, 1357.
(48) Steed, J. W. *Coord. Chem. Rev.* **2001**, *215*, 171.
(49) (a) Rüdiger, V.; Schneider, H.-J.; Solov'ev, V. P.; Kazachenko, V. P.; Raevsky, O. A. *Eur. J. Org. Chem.* **1999**, 1847. (b) Doxsee, K. M.; Wierman, H. R.; Weakley, T. J. R. *J. Am. Chem. Soc.* **1992**, *114*, 5165.
(50) Erk, C.; Zeidler, M. D. *Chem. Phys.* **2004**, *303*, 115.
(51) Leroux, F. *Chem. Bio. Chem.* **2004**, *5*, 644.
(52) Charbonniere, L. J.; Ziessel, R.; Sams, C. A.; Harriman, A. *Inorg. Chem.* **2003**, *42*, 3466.
(53) Harriman, A.; Mayeux, A.; Stroh, C.; Ziessel, R. *Dalton Trans.* **2005**, 2925.
(54) Harriman, A.; Hissler, M.; Ziessel, R. *Phys. Chem. Chem. Phys.* **1999**, *1*, 4203.
(55) (a) Sharp, K.; Honig, B. *Annu. Rev. Biophys. Biochem.* **1990**, *19*, 301. (b) Sitkoff, D.; Sharp, K. A.; Honig, B. *J. Phys. Chem.* **1994**, *98*, 1978. (c) Im, W.; Beglov, D.; Roux, B. *Comput. Phys. Commun.* **1998**, *111*, 59.
(56) Rigby, M.; Smith, E. B.; Wakeman, W. A.; Maitland, G. C. In *The Forces Between Molecules*; Oxford Science Publication, Clarendon Press: Oxford; Chapter 1.

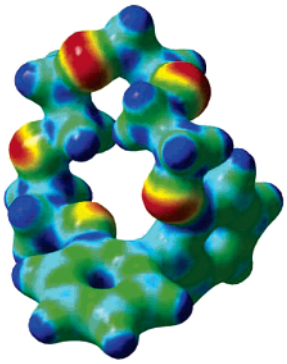

FIGURE 4. Electrostatic potential map for the ground-state conformation of **BPCE5**. The potentials are colored from positive areas in blue to negative areas in red. Note that the phenoxy atoms point into the cavity suitable for metal ion complexation, whereas oxygens in the polyether chain are aligned away from the cavity.

are oriented randomly, as might be expected on the basis of their known flexibility.[40]

Using the partial charges for each atom and the distance from the bound cation, the total electrostatic energy was calculated by a simple summation procedure. Already from the MDS studies, it was observed that several binding sites within the cavity are possible for the Na^+ cation. For simplicity, the first position considered placed the cation close to the biphenyl unit. Calculation of the resulting electrostatic free energy gave a value of $\Delta G_{el} = 7.6$ kJ mol^{-1}, whereas the measured binding energy (ΔG_b) for the uncharged **BPCE5** is -14.0 kJ mol^{-1}.[8] The electrostatic repulsive energy is kept modest by partial charge transfer from the oxygen atoms such that the net charge resident on the bound Na^+ cation is about 0.225 (see the Supporting Information). The computation was repeated with the cation moved to different binding sites and with the magnitude of ΔG_{el} being calculated at each position. As might be expected, ΔG_{el} approaches a minimum as the cation is situated further from the terminals. For example, with the cation placed in the center of the cavity $\Delta G_{el} = 4.4$ kJ mol^{-1} and this falls to $\Delta G_{el} = 2.7$ kJ mol^{-1} when the cation reaches the furthest extreme binding site. In this latter site, which has the cation far removed from the phenoxyl oxygen atoms but still inside the cavity, the calculated electrostatic energy accounts for about 18% of the binding energy measured by fluorescence spectroscopic titration.[8] Although significant, electrostatic repulsion will not prevent formation of the inclusion complex. Similar computations applied to the MDS work[57] indicate that the relative displacement of the bridging unit is restricted by cation binding such that the molecule becomes more rigid. This effect is already known from NMR spectroscopy.[58] There is a corresponding change in the torsion angle for the central connecting bond (Table 1).

Electrochemistry. The redox behavior of the various metal complexes was studied in acetonitrile solution (0.2 M tetra-*N*-butylammonium hexafluorophosphate as background electrolyte) using cyclic voltammetry. The electrochemistry observed for the homotopic and heterotopic complexes is typical for assemblies containing alkynylene-substituted 2,2′:6′,2″-terpyridine ligands in the 4′-position.[59] Thus, the oxidative segment of the cyclic voltammograms recorded for **RCnR** ($n = 1-4$) and **RCEnR** ($n = 4-6$) display a single, quasireversible wave relating to the Ru^{2+}/Ru^{3+} couple at $+1.30$ V vs Ag/AgCl. The redox potentials vary little across the series, indicating that neither the length nor the type of chain perturbs the ground-state electronic properties of the complex. As expected on this basis, the mixed-metal complexes **RCnO** ($n = 1-4$) and **RCEnO** ($n = 4-6$) display two well-separated, quasireversible waves on oxidative scanning that correspond to redox processes taking place at the osmium(II) and ruthenium(II) centers, at $+1.05$ and $+1.35$ V vs Ag/AgCl, respectively. The observed half-wave potentials are in good agreement with related ruthenium(II) and osmium(II) terpyridine complexes.[60] There was no indication for oxidation of the central biphenylene unit under these conditions.

The reductive segment of the cyclic voltammograms recorded for **RCnR** ($n = 1-4$) and **RCEnR** ($n = 4-6$) displayed two obvious peaks. In each case, quasireversible reduction processes are apparent with half-wave potentials of about -1.2 and -1.4 V vs Ag/AgCl. Both processes correspond to two-electron steps, the former process being assigned to the reduction of the ethynylated ligands on the Ru-terpy units and the latter process to reduction of the unsubsituted terpy ligand.[61] The reductive electrochemistry of the mixed-metal complexes is somewhat similar, with quasireversible processes observable at -1.1 and -1.3 V vs Ag/AgCl. Again, both processes correspond to two-electron steps, with the former being assigned to the reduction of the substituted ligands on the metal centers. The more negative reduction potentials are thereby assigned to the terminal parent ligands.

The cyclic voltammograms recorded for **RCEnR** ($n = 4-6$) were unaffected by addition of a large excess of cation (Na^+ and K^+). Although binding is expected to be relatively inefficient under these conditions, there were no indications that occupying the crown ether void affected the redox chemistry of the terminals. It is also important to note that the redox-active terminals remain isolated from each other in electronic terms.

Photophysical Properties. The absorption spectra recorded in acetonitrile at room temperature for **RCnR** ($n = 1-4$) and **RCEnR** ($n = 4-6$) and for the corresponding mixed-metal analogues display characteristic bands associated with bis(2,2′:6′,2″-terpyridine) complexes containing ruthenium(II) and/or osmium(II) centers.[61] As typical examples, the absorption profiles for **RC4R** and **RC4O** are shown in Figure 5. The pronounced metal-to-ligand, charge-transfer (MLCT) absorption transitions for the Ru-terpy and Os-terpy units are centered around 490 nm. The heteroleptic compounds show a pronounced tail stretching out to about 710 nm, which can be assigned to spin-forbidden transitions associated with the osmium-based terminal. The additional bands seen in the near-UV region are assigned to ligand-centered transitions associated with both substituted and parent terpy ligands. The band shapes, absorption maxima, and molar absorption coefficients for the various homoleptic and heteroleptic complexes do not vary significantly across the series. Excitation into the band at 490 nm for the homotopic ruthenium(II) complexes results in the appearance

(57) Reed, T. M.; Gubbins, K. E. In *Applied Statistical Mechanics*; McGraw-Hill: New York, 1973; Chapters 4 and 5.
(58) Wilson, M. J.; Pethrick, R. A.; Pugh, D.; Islam, M. S. *J. Chem. Soc., Faraday Trans.* **1997**, *93*, 2097.
(59) Hissler, M.; Harriman, A.; El-ghayoury, A.; Ziessel, R. *Coord. Chem. Rev.* **1998**, *178*, 1251.
(60) Harriman, A.; Ziessel, R. *Coord. Chem. Rev.* **1998**, *171*, 331.
(61) Sauvage, J.-P.; Collin, J.-P.; Chambron, J.-C.; Guillerez, S.; Coudret, C.; Balzani, V.; Barigelletti, F.; De Cola, L.; Flamigni, L. *Chem. Rev.* **1994**, *94*, 993.

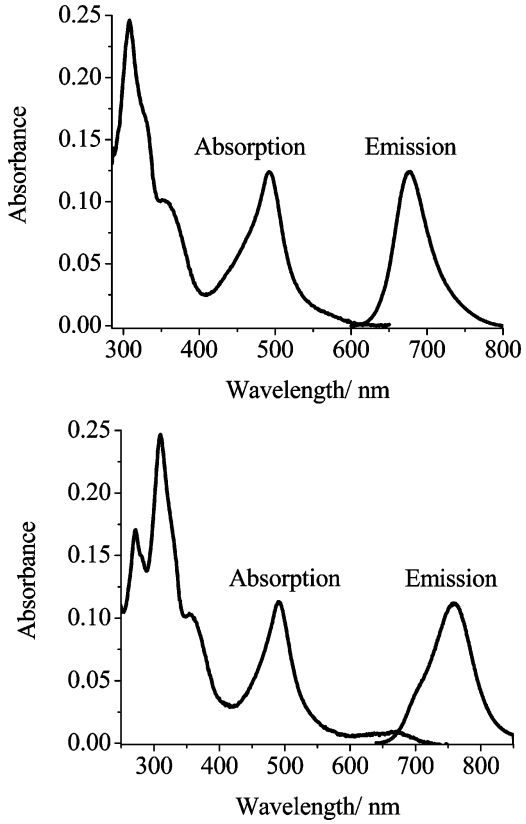

FIGURE 5. Room-temperature absorption and emission spectral profiles recorded for **RC4R** (top) and **RC4O** (bottom) in N_2-purged acetonitrile. Excitation wavelength used in both cases was 490 nm.

of a broad, but very weak, luminescence profile centered at about 675 nm. This emission signal decays via first-order kinetics with a lifetime of around 20 ns, while the emission quantum yield was determined to be 0.004. In contrast, excitation into the 490 nm band for the heteroleptic ruthenium(II)/osmium(II) complexes causes the appearance of an emission profile centered at 760 nm. This latter spectrum bears all the characteristics of emission from an Os-terpy derivative.[62] Again, the emission signal decayed via first-order kinetics, but the derived lifetime was extended to ca. 160 ns. The emission quantum yield was found to be 0.002. It should be noted that the shoulder seen on the higher energy side of the emission profile is most likely due to hot emission from a second MLCT state.[62] In the heteroleptic compounds, there is no obvious indications for emission from the Ru-terpy unit, which is expected around 675 nm, although this chromophore absorbs strongly at 490 nm. It is also notable that the excitation spectrum gives a good match to the absorption spectrum over the entire spectral region. In agreement with previous work,[33,61] these findings are strongly suggestive of quantitative triplet energy transfer from Ru-terpy to Os-terpy in the target compounds.

Importance of Torsion Angle. The main purpose of this investigation is to establish synthetic protocols by which to prepare donor−acceptor dyads in which the electronic conductivity of the bridge can be varied systematically. Although the proposed strategy does not allow synthesis of a planar biphenyl unit, it is possible to produce a wide range of angles using the same general conditions. Further tuning of the torsion angle can

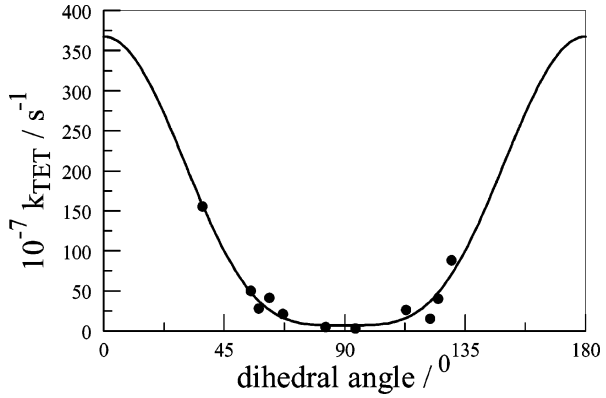

FIGURE 6. Effect of dihedral angle at the central biphenyl bridge on the rate of electron exchange measured in a glassy butyronitrile matrix at low temperature.

be attained by binding a cation to the void provided by crown ether-based straps and this has the added advantage of rigidifying the bridge at ambient temperature. In principle, the range of crown ethers could be extended to include azamacrocycles that bind transition metal cations. This might provide access to derivatives where the geometry could be switched by rapid change in oxidation state of the bound cation.[63] To test the viability of this strategy, we have determined rate constants for triplet energy transfer between the terminals in mixed-metal Ru^{II}/Os^{II} complexes, on the assumption that the geometry remains as derived herein. To favor adoption of the lowest-energy conformation available to the bridge, the complexes were cooled slowly in butyronitrile to below the glass transition temperature. Even in the glassy matrix, the rate constants for through-bond triplet energy transfer are weakly activated because of the disparity between triplet energy gap and accompanying reorganization energy.[14] From a linear Arrhenius-type plot, however, it is possible to determine the activationless rate constant (k_{TET}) for intramolecular triplet−triplet energy transfer.[33]

In the glassy matrix, there is a smooth correlation between k_{TET} and the dihedral angle (ϕ) for the central biphenyl unit (Figure 6).[14] The rate of triplet energy transfer, which is due solely to electron exchange, reaches a minimum at 90° and is maximal when the biphenyl bridge is planar. This effect is related to the degree of electronic conductivity across the bridge. The general effect is similar to that observed previously for hole transfer in the corresponding mixed-valence Ru^{III}/Ru^{II} complexes[5c] but differs from the angle dependence found for light-induced electron transfer in bridged bis-porphyrins.[3a] In this latter case the optimum angle for intramolecular electron transfer was about 45°. The close agreement between the angle dependence for triplet-energy transfer and hole transfer can be used to argue that the former process is limited by hole transfer through the bridging HOMO.

$$k_{TET} = k_N + k_0(\cos^2 \phi)^n \quad (1)$$

In quantitative terms, the variation in k_{TET} between coplanar and orthogonal geometries is a factor of ca. 50-fold. It should be noted, however, that k_{TET} values remain relatively constant over a wide range of angles at the bottom of the well, as depicted in Figure 6. This arises because the k_{TET} depends on the square

(62) Benniston, A. C.; Harriman, A.; Li, P.; Sams, C. A. *J. Phys. Chem. A.* **2005**, *109*, 2302.

(63) Fabbrizzi, L.; Licchelli, M.; Pallavicini, P. *Acc. Chem. Res.* **1999**, *32*, 846.

of the dihedral angle term. The major increase in k_{TET} occurs when the dihedral angle becomes less than 45°; thus, between $\phi = 45°$ and $\phi = 10°$ there is a large variation in rate. Such behavior is highly promising for the design of molecular-scale switches based on biphenyl rotors, especially since it is not necessary to switch the conformation by 90°. For example, one could envisage using a small dihedral angle in a biphenyl unit to promote rapid electron migration in one direction. A triggered twist in the biphenyl to a larger dihedral angle would retard the return charge recombination.[64]

Electron exchange at 90° ($k_{TET} = 7.1 \times 10^6$ s^{-1}) can be attributed to nuclear tunneling through the connecting σ-bond. In contrast, electron exchange in the (hypothetical) coplanar geometry ($k_{TET} = 3.6 \times 10^8$ s^{-1}) is dominated by super-exchange interactions between the phenylene rings. The kinetic data collected at intermediate angles can be well described in terms of eq 1 where k_N refers to the rate constant for nuclear tunneling and k_0 is the rate constant for electron exchange across the coplanar bridge. The coefficient *n*, which is expected to possess a numerical value of $n = 2$ for through-bond triplet energy transfer, is calculated from the nonlinear least-squares best fit to be 1.95. The results, therefore, are entirely consistent with the proposed mechanism and with the concept that the dihedral angle is a controlling feature in the reaction dynamics. Triplet energy transfer in fluid solution at ambient temperature follows a similar trend, although the k_{TET} values are higher at any given angle, and eq 1 is obeyed. A more rigorous analysis is warranted, however, to allow for fluxional variations in the geometry of the bridge. These findings will be published at a later date.

Experimental Section

General experimental methods are reported in the Supporting Information. Preparations reported below were carried out under a N_2 atmosphere unless otherwise stated.

When performing computational studies, it was recognized that high-level calculations performed on the entire complexes, including the two large metal ions, would be computationally very demanding. Therefore, it was decided to perform most studies on molecules **Cn** ($n = 1-4$) and **CEn** ($n = 4-6$) with terminal pyridine units as opposed to terpyridine. The Gaussian 03 program[65] was used to perform these calculations, utilizing the semiempirical PM3 method.[66] The Polack−Ribiere algorithm was used to a maximum energy gradient of 0.01 kcal/(Å mol). Several geometry optimizations were carried out on the molecules **Cn** ($n = 1-4$) and **CEn** ($n = 4-6$) starting from different initial structures,[67] selected using the so-called tree-search algorithm.[68] All calculations were run *in vacuo*. Confirmation of the location of a global minimum was obtained by the appearance of zero imaginary frequencies. Related work was carried out with selected binuclear complexes in order to ensure that the geometry of the connector remained essentially unaffected by the nature of the terminal groups.

Gaussian 03[65] was also used to perform a scan calculation whereby the central dihedral angle in 2,2′-dimethoxybiphenyl was rotated through 180°. At 2° intervals, the dihedral angle was constrained and the rest of the structure was minimized using the DFT method B3LYP and a 6-31G(d) basis set. The total energy was thereby computed as a function of torsion angle. Determination of the minimum energy conformation and molecular dynamics simulations on the full molecules, **RCnR** ($n = 1,4$) and **RCEnR** ($n = 4-6$), were performed using the Discover module within Insight II[69] running on a Silicon Graphics O2+ machine. Potentials were assigned to the atom types in the molecules using a modified ESFF force field.[70] Minimum energy conformations were then calculated using both the conjugate gradient method and a truncated Newton method, starting from many different initial geometries.[67] Calculations were performed in vacuo for all molecules. Molecular dynamics simulations (MDS) were also performed in vacuo, using the minimum energy conformation as a starting point, CHARMM with stochastic boundary conditions. These MDS studies were setup in two stages, with 10 ps of equilibration time and 20 ps of run time, with the temperature being set at 295 ± 5 K. A comprehensive set of data was saved every 10 fs of simulation. Calculations on several molecules were also performed in a solvent box containing approximately 1500 water molecules and the appropriate number of counterions. It was observed that there was very little difference between the results obtained in vacuo and those collected for a continuum solvent box. The minimum energy conformations were remarkably similar, but inspection of the MDS indicated damping of internal motions when in a solvent box. The values reported in Table 1 refer to those extracted from the calculations performed in vacuo.

I. General Procedure for the Synthesis of 1a−g. To a solution of ca. 2 mmol of 4,4′-diiodo-2,2′-biphenol in DMF (40 mL) was added 2.6 equiv of K_2CO_3. The mixture was stirred at 90 °C for 1.5 h. Then, 1.2 equiv of ditosylate linker (or CH_2I_2) in DMF (40 mL) was added slowly. After the mixture was heated at 90 °C for ∼24 h, the solution was cooled and the DMF removed. The residue was extracted with ethyl acetate, which was washed with H_2O, separated, and dried over $MgSO_4$. Removal of the solvent afforded the crude product, which was purified by column chromatography.

1b: 0.8 g (1.8 mmol) of 4,4′-diiodo-2,2′-biphenol, 0.75 g (2.0 mmol) of ethylene di-*p*-tosylate; silica, petroleum ether/ethyl acetate 8/1; yield 0.55 g (65%) white solid; ^{1}H NMR (δ, 300 MHz, $CDCl_3$) 4.05 (d, br, $J = 8.6$ Hz, 2H), 4.45 (d, br, $J = 8.6$ Hz, 2H), 7.03 (d, $J = 7.9$ Hz, 2H), 7.53−7.57 (d and dd, $J = 7.9$ Hz, $J = 1.6$ Hz, 4H); EI-MS (*m*/*z*) 464 (calcd $M_r = 463.88$ for $C_{14}H_{10}O_2I_2$).

1c: 0.8 g (1.8 mmol) of 4,4′-diiodo-2,2′-biphenol, 0.84 g (2.2 mmol) of 1,3-ditosylpropane; silica, petroleum ether/ethyl acetate 4/1; yield 0.48 g (55%) white solid; ^{1}H NMR (δ, 300 MHz, $CDCl_3$) 2.03 (quintet, $J = 5.2$ Hz, 2H), 4.35 (s, br, 4H), 6.96 (d, $J = 7.8$ Hz, 2H), 7.45−7.48 (m, 4H); EI-MS (*m*/*z*) 478 (calcd $M_r = 477.89$ for $C_{15}H_{12}O_2I_2$).

1d: 0.8 g (1.8 mmol) of 4,4′-diiodo-2,2′-biphenol, 0.87 g (2.2 mmol) of 1,4-ditosylbutane; silica, petroleum ether/ethyl acetate 5/1; yield 0.56 g (62%) white solid; ^{1}H NMR (δ, 300 MHz, $CDCl_3$) 1.91 (m, br, 4H), 4.13 (m, br, 2H), 4.47 (m, br, 2H), 6.96 (d, $J =$

(64) Benniston, A. C.; Harriman, A. *Chem. Soc. Rev.* **2006**, *35*, 169.
(65) Gaussian 03, Revision C.02: Frisch, M. J.; Trucks, G. W.; Schlegel, H. B.; Scuseria, G. E.; Robb, M. A.; Cheeseman, J. R.; Montgomery, J. A., Jr.; Vreven, T.; Kudin, K. N.; Burant, J. C.; Millam, J. M.; Iyengar, S. S.; Tomasi, J.; Barone, V.; Mennucci, B.; Cossi, M.; Scalmani, G.; Rega, N.; Petersson, G. A.; Nakatsuji, H.; Hada, M.; Ehara, M.; Toyota, K.; Fukuda, R.; Hasegawa, J.; Ishida, M.; Nakajima, T.; Honda, Y.; Kitao, O.; Nakai, H.; Klene, M.; Li, X.; Knox, J. E.; Hratchian, H. P.; Cross, J. B.; Bakken, V.; Adamo, C.; Jaramillo, J.; Gomperts, R.; Stratmann, R. E.; Yazyev, O.; Austin, A. J.; Cammi, R.; Pomelli, C.; Ochterski, J. W.; Ayala, P. Y.; Morokuma, K.; Voth, G. A.; Salvador, P.; Dannenberg, J. J.; Zakrzewski, V. G.; Dapprich, S.; Daniels, A. D.; Strain, M. C.; Farkas, O.; Malick, D. K.; Rabuck, A. D.; Raghavachari, K.; Foresman, J. B.; Ortiz, J. V.; Cui, Q.; Baboul, A. G.; Clifford, S.; Cioslowski, J.; Stefanov, B. B.; Liu, G.; Liashenko, A.; Piskorz, P.; Komaromi, I.; Martin, R. L.; Fox, D. J.; Keith, T.; Al-Laham, M. A.; Peng, C. Y.; Nanayakkara, A.; Challacombe, M.; Gill, P. M. W.; Johnson, B.; Chen, W.; Wong, M. W.; Gonzalez, C.; Pople, J. A. Gaussian, Inc., Wallingford CT, 2004.
(66) (a) Trucks, G. W.; Salter, E. A.; Sosa, C.; Bartlett, R. J. *Chem. Phys. Lett.* **1988**, *147*, 359. (b) Trucks, G. W.; Watts, J. D.; Salter, E. A.; Bartlett, R. J. *Chem. Phys. Lett.* **1988**, *153*, 490.
(67) Saunders, M.; Houk, K. N.; Wu, Y.-D.; Still, W. C.; Lipton, M.; Chang, G.; Guida, W. C. *J. Am. Chem. Soc.* **1990**, *112*, 1419.
(68) Lipton, M.; Still, W. C. *J. Comput. Chem.* **1988**, *9*, 343.
(69) Accelrys Software Inc., San Diego, CA.
(70) Shi, S.; Yan, L.; Yang, Y.; Fisher-Shaulsky, J.; Thatcher, T. *J. Comput. Chem.* **2003**, *24*, 1059.
(71) Suen, H. F.; Wilson, S. W.; Pomerantz, M.; Walsh, J. L. *Inorg. Chem.* **1989**, *28*, 786.

8.0 Hz, 2H), 7.36 (d, J = 1.6 Hz, 2H), 7.39 (dd, J = 8.0 Hz, J = 1.6 Hz); EI-MS (m/z) 492 (calcd M_r = 491.91 for $C_{16}H_{14}O_2I_2$).

1e: 1.0 g (2.44 mmol) of 4,4′-diiodo-2,2′-biphenol, 1.44 g (2.93 mmol) of tri(ethylene glycol) di-*p*-tosylate; silica, petroleum ether/ethyl acetate (1:1) followed by petroleum ether/ethyl acetate (9:1); yield 0.4 g (30%) white solid; ^{1}H NMR (δ, 300 MHz; $CDCl_3$) 3.50 (4H, s), 3.90−3.60 (6H, m), 4.2 (2H, m), 6.75 (d, J = 7.8 Hz, 2H), 7.20 (d,, J = 1.5 Hz, 2H), 7.27 (dd, J = 7.8 Hz, J = 1.5 Hz, 2H); EI-MS (m/z) 551.93 (calcd M_r = 551.39 for $C_{18}H_{18}O_4I_2$).

1f: 0.8 g (1.8 mmol) of 4,4′-diiodo-2,2′-biphenol, 1.1 g (2.2 mmol) of tetra(ethylene glycol) di-*p*-tosylate; alumina, petroleum ether/ethyl acetate 3/1; yield 0.39 g (36%) white solid; ^{1}H NMR (δ, 300 MHz, $CDCl_3$) 3.54−3.71 (m, 8H), 3.73−3.83 (m, 4H), 3.95−4.01 (m, 2H), 4.13−4.21 (m, 2H), 6.85 (d, J = 7.8 Hz, 2H), 7.29 (d, J = 1.5 Hz, 2H), 7.33 (dd, J = 7.8 Hz, J = 1.5 Hz, 2H); EI-MS (m/z) 596 (calcd M_r = 595.96 for $C_{20}H_{22}O_5I_2$).

1g: 1.0 g (2.3 mmol) of 4,4′-diiodo-2,2′-biphenol, 1.7 g (3.1 mmol) of penta(ethylene glycol) di-*p*-tosylate; silica, ether/petroleum ether 9/1; yield 0.53 g (36%) white solid;. ^{1}H NMR (δ, 300 MHz, $CDCl_3$) 3.55−3.74 (m, 16H), 4.01−4.17 (m, 4H), 6.88 (d, J = 7.8 Hz, 2H), 7.30 (d, J = 1.5 Hz, 2H), 7.33 (dd, J = 7.8 Hz, J = 1.5 Hz, 2H); EI-MS (m/z) 640 (calcd M_r = 639.98 for $C_{22}H_{26}O_6I_2$).

II. General Procedure for the Synthesis of C1−C4 and CE5. A mixture of ^{i}Pr$_2$NH (20 mL)/THF (50 mL) was used to dissolve 0.44−0.65 mmol of **1x** (**x** = **a**, **b**, **c**, **d**, and **f**) and 6 mol % of $Pd(PPh_3)_4$. Then, 1.15 equiv of 4′-ethynyl-terpy **2** was added. The mixture was stirred at rt until **2** was fully dissolved and was then heated at reflux overnight. After the reaction was complete (monitored by TLC), the mixture was cooled to rt and filtered. The filtrate was evaporated to dryness. The residue was extracted with CH_2Cl_2, which was washed with H_2O, separated, and dried over $MgSO_4$. The crude product was purified by column chromatography (except **C1**, which is too insoluble to be columned. It was purified by washing repeatedly with ethyl acetate, ethanol, water and ether).

C1: 0.20 g (0.44 mmol) of **1a**; yield 0.155 g (49%) off-white solid; ^{1}H NMR (δ, 300 MHz, $CDCl_3$) 5.66 (s, 2H), 7.36−7.40 (m, 6H), 7.44 (dd, J = 8.2 Hz, J = 1.7 Hz, 2H), 7.73 (d, J = 8.2 Hz, 2H), 7.90 (td, J = 7.8 Hz, J = 1.8 Hz, 4H), 8.61 (s, 4H), 8.64 (m, 4H), 8.75 (m, 4H). ^{13}C{^{1}H} NMR (δ, 500 MHz, $CDCl_3$) 98.4 (C of methylene); 88.9, 92.6 (C of −C≡C−); 121.3, 122.9, 123.3, 124.1, 124.3, 127.9, 128.7, 128.9, 133.1, 136.9, 149.2, 155.5, 155.63, 155.67; EI-MS (m/z) 708 (calcd M_r = 708.23 for $C_{47}H_{28}N_6O_2$). Anal. Calcd for $C_{47}H_{28}N_6O_2\cdot H_2O$: C, 77.67; H, 4.16; N, 11.56. Found: C, 77.68; H, 4.09; N, 11.53.

C2: 0.30 g (0.65 mmol) of **1b**; basic alumina, CH_2Cl_2; yield 0.19 g (41%) off-white solid; ^{1}H NMR (δ, 300 MHz, $CDCl_3$) 4.16 (d, br, 2H), 4.54 (d, br, 2H), 7.36 ∼ 7.47 (m, 10H), 7.90 (td, J = 7.7 Hz, J = 1.5 Hz), 8.62 (s, 4H), 8.66 (m, 4H), 8.75 (m, 4H); ^{13}C{^{1}H} NMR (δ, 500 MHz, $CDCl_3$) 73.3 (C of ethylene); 88.6, 93.2 (C of −C≡C-); 121.5, 123.1, 124.2, 124.3, 126.3, 128.5, 130.8, 132.7, 133.5, 137.2, 149.5, 155.8, 155.9, 158.1; EI-MS (m/z) 722 (calcd M_r = 722.24 for $C_{48}H_{30}N_6O_2$). Anal. Calcd for $C_{48}H_{30}N_6O_2\cdot H_2O$: C, 77.82; H, 4.35; N, 11.34. Found: C, 78.06; H, 3.78; N, 11.27.

C3: 0.25 g (0.52 mmol) of **1c**; basic alumina, CH_2Cl_2; yield 0.217 g (56%) off-white solid; ^{1}H NMR (δ, 300 MHz, $CDCl_3$) 2.12 (m, 2H), 4.46 (t, J = 5.0 Hz, 4H), 7.31 ∼ 7.41 (m, 10H), 7.90 (td, J = 7.7 Hz, J = 1.8 Hz, 4H), 8.62 (s, 4H), 8.65 (m, 4H), 8.75 (m, 4H); ^{13}C{^{1}H} NMR (δ, 500 MHz, $CDCl_3$) 29.8, 71.4 (C of methylene); 88.0, 93.6 (C of −C≡C−); 121.2, 121.3, 122.9, 123.0, 124.0, 126.9, 130.0, 132.7, 133.1, 136.9, 149.2, 155.6, 155.7, 157.1; EI-MS (m/z) 736 (calcd M_r = 736.26 for $C_{49}H_{32}N_6O_2$). Anal. Calcd for $C_{49}H_{32}N_6O_2\cdot H_2O$: C, 77.97; H, 4.54; N, 11.11. Found: C, 77.76; H, 4.12; N, 11.01.

C4: 0.32 g (0.65 mmol) of **1d**; basic alumina, CH_2Cl_2; yield 0.16 g (33%) off-white solid; ^{1}H NMR (δ, 300 MHz, $CDCl_3$) 2.02 (m, br, 4H), 4.26 (m, br, 2H), 4.56 (m, br, 2H), 7.29−7.41 (m, 10H), 7.91 (td, J = 7.9 Hz, J = 1.8 Hz, 4H), 8.61 (s, 4H), 8.66 (m, 4H), 8.75 (m, 4H); ^{13}C{^{1}H} NMR (δ, 500 MHz, $CDCl_3$) 27.5, 71.6 (C of methylene); 88.0, 94.0 (C of −C≡C−); 119.4, 121.5, 123.0, 123.1, 124.2, 125.7, 130.3, 131.3, 133.6, 137.3, 149.3, 155.59, 155.73, 157.2; EI-MS (m/z) 750 (calcd M_r = 750.27 for $C_{50}H_{34}N_6O_2$). Anal. Calcd for $C_{50}H_{34}N_6O_2\cdot H_2O$: C, 78.11; H, 4.72; N, 10.93. Found: C, 78.52; H, 4.43; N, 10.93.

CE5: 0.34 g (0.57 mmol) of **1f**; basic alumina, ethyl acetate/petroleum ether 1/2; yield 0.21 g (43%) off-white crystals; ^{1}H NMR (δ, 300 MHz, $CDCl_3$) 3.60−3.74 (m, 8H), 3.83−3.87 (m, 4H), 4.05−4.16 (m, 2H), 4.26−4.33 (m, 2H), 7.21−7.25 (m, 6H), 7.38 (ddd, J = 7.5 Hz, J = 4.8 Hz, J = 1.2 Hz, 4H), 7.90 (td, J = 7.7 Hz, J = 1.8 Hz, 4H), 8.62 (s, 4H), 8.65 (m, 4H), 8.75 (m, 4H); ^{13}C{^{1}H} NMR (δ, 500 MHz, $CDCl_3$) 68.4, 69.9, 71.3, 71.4 (C of ethylene); 87.7, 94.3 (C of −C≡C−); 115.5, 121.5, 122.9, 123.1, 124.3, 124.6, 129.5, 131.5, 133.7, 17.2, 149.5, 155.8, 156.0, 156.6; EI-MS (m/z) 854 (calcd M_r = 854.32 for $C_{54}H_{42}N_6O_5$). Anal. Calcd for $C_{54}H_{42}N_6O_5$: C, 75.86; H, 4.95; N, 9.83. Found: C, 75.99; H, 4.95; N, 9.80.

III. General Procedure for the Synthesis of RCnR and RCE5R (n = 1, 2, 3). A mixture of acetone (40 mL)/methanol (20 mL)/chloroform (20 mL) was used to dissolve 2.2 equiv of $[Ru(tpy)(CH_3CN)_3](PF_6)_2$. To this mixture held at reflux temperature was added a solution of 30 mg (ca. 4×10^{-5} mol) of **C1**−**C3** or **CE5** in chloroform (40 mL) dropwise over 1 day. Additional chloroform (20 mL) was added. The red mixture was refluxed for about 1 week. Upon cooling to rt, the mixture was filtered and the resultant solid washed with acetonitrile. The combined filtrates were reduced in volume to ca. 20 mL, and 0.15 g KPF_6 in H_2O (5 mL) was added dropwise. The resultant precipitate was filtered and washed with H_2O and ether. The crude product was purified by silica column chromatography (CH_3CN/H_2O/satd KNO_3 90/15/1).

RC1R: 70 mg (9.4×10^{-5} mol) of $Ru(tpy)(CH_3CN)_3](PF_6)_2$; 30 mg ($4.2 \times 10^{-5}$ mol) of **C1**; yield 45 mg (54%) red powder; ^{1}H NMR (δ, 500 MHz, CD_3CN) 5.82 (s, 2H), 7.20−7.26 (m, 8H), 7.41−7.44 (m, 8H), 7.66 (d, J = 1.8 Hz, 2H), 7.75 (dd, J = 8.1 Hz, J = 1.8 Hz, 2H), 7.96−8.02 (m, 8H), 8.08 (d, J = 8.1 Hz, 2H), 8.48 (t, J = 8.3 Hz, 2H), 8.53−8.58 (m, 8H), 8.81 (d, J = 8.3 Hz, 4H), 8.94 (s, 4H); MALDI-TOF (matrix: DITHRANOL) (m/z) 1668.3 (calcd 1668.2 for $[M - 2PF_6]^+$), 1523.4 (calcd 1523.2 for $[M - 3PF_6]^+$), 1377.4 (calcd 1377.2 for $[M - 4PF_6]^+$), 1043.3 (calcd 1043.2 for $[M - Ru(tpy) - 4PF_6]^+$), 688.7 (calcd 688.6 for $[M - 4PF_6]^{2+}$). Anal. Calcd for $Ru_2C_{77}H_{50}N_{12}O_2\cdot P_4F_{24}\cdot H_2O$: C, 46.82; H, 2.65; N, 8.51. Found: C, 46.78; H, 2.46; N, 8.65.

RC2R: 68 mg (9.1×10^{-5} mol) of $Ru(tpy)(CH_3CN)_3](PF_6)_2$; 30 mg ($4.15 \times 10^{-5}$ mol) **C2**; yield 33 mg (40%) red powder; ^{1}H NMR (δ, 500 MHz, CD_3CN) 4.26 (d, br, 2H), 4.66 (d, br, 2H), 7.20−7.26 (m, 8H), 7.41−7.45 (m, 8H), 7.66 (d, J = 7.6 Hz, 2H), 7.69 (d, J = 1.5 Hz, 2H), 7.74 (dd, J = 7.6 Hz, J = 1.5 Hz, 2H), 7.96−8.02 (m, 8H), 8.48 (t, J = 8.3 Hz, 2H), 8.54−8.57 (m, 8H), 8.81 (d, J = 8.3 Hz, 4H), 8.94 (s, 4H); MALDI-TOF (matrix: DITHRANOL) (m/z) 1537.4 (calcd 1537.2 for $[M - 3PF_6]^+$), 1391.4 (calcd 1391.2 for $[M - 4PF_6]^+$), 1057.4 (calcd 1057.2 for $[M - Ru(tpy) - 4PF_6]^+$), 696.2 (calcd 696.1 for $[M - 4PF_6]^{2+}$). Anal. Calcd for $Ru_2C_{78}H_{52}N_{12}O_2\cdot P_4F_{24}\cdot 3H_2O$: C, 46.25; H, 2.89; N, 8.30. Found: C, 46.00; H, 3.02; N, 8.37.

RC3R: 67 mg (9.0×10^{-5} mol) of $[Ru(tpy)(CH_3CN)_3](PF_6)_2$; 30 mg ($4.1 \times 10^{-5}$ mol) **C3**; yield 35 mg (43%) red powder; ^{1}H NMR (δ, 500 MHz, CD_3CN) 2.1 (buried under H_2O signal, 2H), 4.58 (t, J = 5.1 Hz, 4H), 7.20−7.26 (m, 8H), 7.41−7.45 (m, 8H), 7.56 (d, J = 7.6 Hz, 2H), 7.64 (dd, J = 7.6 Hz, J = 1.5 Hz, 2H), 7.67 (d, J = 1.5 Hz, 2H), 7.96−8.02 (m, 8H), 8.47 (t, J = 8.2 Hz, 2H), 8.54−8.57 (m, 8H), 8.81 (d, J = 8.2 Hz, 4H), 8.93 (s, 4H); MALDI-TOF (matrix: DCTB) (m/z) 1841.4 (calcd 1841.2 for $[M - PF_6]^+$), 1216.4 (calcd 1216.2 for $[M - Ru(tpy) - 3PF_6]^+$). Anal. Calcd for $Ru_2C_{79}H_{54}N_{12}O_2\cdot P_4F_{24}$: C, 47.79; H, 2.74; N, 8.47. Found: C, 47.53; H, 2.94; N, 8.44.

RCE5R: 60 mg (8.0×10^{-5} mol) $Ru(tpy)(CH_3CN)_3](PF_6)_2$; 30 mg ($3.5 \times 10^{-5}$ mol) of **CE5**; yield 45 mg (61%) red powder; ^{1}H NMR (δ, 500 MHz, CD_3CN) 3.63−3.71 (m, 8H), 3.86−3.90 (m,

4H), 4.20−4.24 (m, 2H), 4.41−4.46 (m, 2H), 7.20−7.26 (m, 8H), 7.40−7.45 (m, 10H), 7.51 (dd, J = 7.6 Hz, J = 1.5 Hz, 2H), 7.54 (d, J = 1.5 Hz, 2H), 7.96−8.02 (m, 8H), 8.48 (t, J = 8.2 Hz, 2H), 8.51−8.58 (m, 8H), 8.81 (d, J = 8.2 Hz, 4H), 8.94 (s, 4H). MALDI-TOF (matrix: DCTB) (*m*/*z*) 1959.5 (calcd 1959.2 for $[M - PF_6]^+$), 1334.5 (calcd 1334.3 for $[M - Ru(tpy) - 3PF_6]^+$). Anal. Calcd for $Ru_2C_{84}H_{64}N_{12}O_5 \cdot P_4F_{24} \cdot 2H_2O$: C, 47.16; H, 3.20; N, 7.86. Found: C, 47.03; H, 2.81; N, 7.81.

IV. General Procedure for the Synthesis of 5a−g. A mixture of $^iPr_2NH$ (15 mL)/THF (40 mL)/CH_3CN (20 mL) was used to dissolve 2.4 × 10^{-4}−4.4 × 10^{-4} mol **1x** (**x** = **a**−**g**), 10 mol % of $Pd(PPh_3)_2Cl_2$ and 20 mol % of CuI. After this yellow mixture was brought to reflux, 1.0 equiv of [Ru(terpy)(4′-ethynyl-terpy)]$(PF_6)_2$] **4** in CH_3CN (40 mL) was added over 1 day via a syringe pump. The mixture was held at reflux for an additional 1 day. The deep red mixture was evaporated to dryness. The residue was redissolved in CH_3NO_2 and filtered. The CH_3NO_2 filtrate was washed with dilute HCl, Na_2CO_3 (aq), and water, separated, and dried over $MgSO_4$. The crude product was purified by silica column chromatography using CH_3CN/H_2O/saturated KNO_3 (90/14/1) as the eluent. The combined collections of the desired product were reduced in volume, and KPF_6 aqueous solution added to precipitate the product. The red solid was filtered, washed with H_2O and ether, and dried in vacuo. The corresponding binuclear ruthenium(II) complexes **RCnR** (n = 1−4) and **RCEnR** (n = 4−6) were isolated as a minor product.

5b: 0.20 g (4.3 × 10^{-4} mol) of **1b**; yield 108 mg (20%); ^{1}H NMR (δ, 300 MHz, CD_3CN) 4.14 (br, 2H), 4.57 (br, 2H), 7.18−7.25 (m, 5H), 7.38−7.43 (m, 4H), 7.54−7.72 (m, 5H), 7.97 (m, 4H), 8.46 (t, J = 8.1 Hz, 1H), 8.53 (m, 4H), 8.79 (d, J = 8.1 Hz, 2H), 8.91 (s, 2H); ESI-MS (*m*/*z*) 1073.1 (calcd 1073.0 for $[M - PF_6]^+$), 464.1 (calcd 464.0 for $[M - 2PF_6]^{2+}$). Minor product **RC2R**: yield 89 mg; ^{1}H NMR and MALDI-MS, see section III.

5c: 0.15 g (3.1 × 10^{-4} mol) of **1c**; yield 163 mg of (42%); ^{1}H NMR (δ, 300 MHz, CD_3CN) 2.07 (quintet, br, 2H), 4.43 (t, br, 2H), 4.50 (t, br, 2H), 7.12 (d, J = 8.0 Hz, 1H), 7.18−7.24 (m, 4H), 7.38−7.46 (m, 5H), 7.55−7.66 (m, 4H), 7.97 (m, 4H), 8.46 (t, J = 8.1 Hz, 1H), 8.53 (m, 4H), 8.79 (d, J = 8.1 Hz, 2H), 8.91 (s, 2H); ESI-MS (*m*/*z*) 1087.2 (calcd 1087.0 for $[M - PF_6]^+$), 471.2 (calcd 471.0 for $[M - 2PF_6]^{2+}$). Minor product **RC3R**: yield 101 mg; ^{1}H NMR and MALDI-MS, see section III.

5d: 0.20 g (4.1 × 10^{-4} mol) of **1d**; yield 102 mg (20%); ^{1}H NMR (δ, 300 MHz, CD_3CN) 1.9 (overlapped with CD_3CN signal, m, br, 4H), 4.27 (m, 2H), 4.57 (m, 2H), 7.13 (d, J = 8.0 Hz, 1H), 7.18−7.24 (m, 4H), 7.38−7.44 (m, 4H), 7.47−7.57 (m, 5H), 7.97 (m, 4H), 8.46 (t, J = 8.1 Hz, 1H), 8.53 (m, 4H), 8.79 (d, J = 8.1 Hz, 2H), 8.91 (s, 2H); ESI-MS (*m*/*z*) 1101.1 (calcd 1101.1 for $[M - PF_6]^+$), 478.0 (calcd 478.0 for $[M - 2PF_6]^{2+}$). Minor product **RC4R**: yield 79 mg; ^{1}H NMR (δ, 500 MHz, CD_3CN) 1.9 (buried under CD_3CN signal, 4H), 4.40 (t, br, 2H), 4.70 (m, br, 2H), 7.21−7.26 (m, 8H), 7.41−7.45 (m, 8H), 7.58−7.61 (m, 6H), 7.96−8.02 (m, 8H), 8.48 (t, J = 8.3 Hz, 2H), 8.54−8.57 (m, 8H), 8.81 (d, J = 8.3 Hz, 4H), 8.94 (s, 4H). MALDI-TOF (matrix: DCTB) (*m*/*z*) 1855.1 (calcd 1855.2 for $[M - PF_6]^+$), 855.1 (calcd 854.8 for $[M - 2PF_6]^{2+}$). Anal. Calcd for $Ru_2C_{80}H_{56}N_{12}O_2 \cdot P_4F_{24} \cdot 2H_2O$: C, 47.21; H, 2.97; N, 8.26. Found: C, 47.38; H, 2.90; N, 8.15.

5e: 0.17 g, (3.1 × 10^{-4} mmol) of **1e**; yield 60 mg (15%); ^{1}H NMR (δ, 300 MHz, CD_3CN) 3.58−3.43 (m, 4H), 4.05−3.71 (m, 6H), 4.44−4.3 (m, 2H), 6.96 (d, J = 7.9 Hz, 1H), 7.3−7.2 (m, 4H), 7.40 (m, 9H, 4H), 7.95 (m, 4H), 8.90 (s, 2H), 8.46 (t, J = 8.1 Hz, 1H), 8.53 (m, 4H), 8.78 (d, J = 8.1 Hz, 2H); ESI (*m*/*z*) 1161.3 (calcd 1161.1 for $[M - PF_6]$). Minor product **RuL$_5$Ru**: yield 65 mg. Anal. Calcd for $RuC_{50}H_{39}N_6IP_2F_{12} \cdot 4H_2O$: C, 43.59; H, 3.44; N, 6.10. Found: C, 43.02; H, 2.63; N, 5.94%

5f: 0.15 g (2.4 × 10^{-4} mol) of **1f**; yield 101 mg (30%); ^{1}H NMR (δ, 300 MHz, CD_3CN) 3.56−3.67 (m, 8H), 3.75−3.86 (m, 4H), 4.04−4.17 (m, 2H), 4.24−4.38 (m, 2H), 7.00 (d, J = 7.8 Hz, 1H), 7.18−7.25 (m, 4H), 7.33−7.49 (m, 9H), 7.97 (m, 4H), 8.47 (t, J = 8.1 Hz, 1H), 8.53 (m, 4H), 8.79 (d, J = 8.1 Hz, 2H), 8.92 (s, 2H); ESI-MS (*m*/*z*) 1205.3 (calcd 1205.1 for $[M - PF_6]^+$), 1059.2 (calcd 1059.9 for $[M - 2PF_6]^+$), 530.0 (calcd 530.1 for $[M - 2PF_6]^{2+}$). Minor product **RCE5R**: yield 33 mg; ^{1}H NMR and MALDI-MS, see section III.

5g: 0.22 g (3.4 × 10^{-4} mol) of **1g**; yield 130 mg (27%); ^{1}H NMR (δ, 300 MHz, CD_3CN) 3.56−3.65 (m, 12H), 3.68−3.75 (m, 4H), 3.97−4.10 (m, 2H), 4.28−4.44 (m, 2H), 7.03 (d, J = 7.9 Hz, 1H), 7.20−7.26 (m, 4H), 7.35−7.56 (m, 9H), 7.98 (m, 4H), 8.48 (t, J = 8.1 Hz, 1H), 8.56 (m, 4H), 8.81 (d, J = 8.1 Hz, 2H), 8.92 (s, 2H); ESI-MS (*m*/*z*) 1249.1 (calcd 1249.2 for $[M - PF_6]^+$), 552.1 (calcd 552.1 for $[M - 2PF_6]^{2+}$). Minor product **RCE6R**: yield 36 mg; ^{1}H NMR (δ, 500 MHz, CD_3CN) 3.61−3.68 (m, 12H), 3.85 (m, 4H), 4.26−4.30 (m, 2H), 4.40−4.45 (m, 2H), 7.21−7.26 (m, 8H), 7.41−7.46 (m, 8H), 7.49 (d, J = 7.6 Hz, 2H), 7.52 (dd, J = 7.6 Hz, J = 1.2 Hz, 2H), 7.58 (d, J = 1.2 Hz, 2H), 7.96−8.02 (m, 8H), 8.48 (t, J = 8.2 Hz, 2H), 8.53−8.58 (m, 8H), 8.81 (d, J = 8.2 Hz, 4H), 8.94 (s, 4H); MALDI-TOF (matrix: DCTB) (*m*/*z*) 2187.2 (calcd 2187.2 for $[M + K]^+$), 2003.3 (calcd 2003.2 for $[M - PF_6]^+$), 1859.3 (calcd 1857.7 for $[M - PF_6]^+$), 928.7 (calcd 928.8 for $[M - 2PF_6]^{2+}$). Anal. Calcd for $Ru_2C_{86}H_{68}N_{12}O_6 \cdot P_4F_{24} \cdot 3H_2O$: C, 46.92; H, 3.39; N, 7.63. Found: C, 46.76; H, 3.06; N, 7.50.

V. General Procedure for the Synthesis of RCnO (n = 1−4), RCE4O, RCE5O, and RCE6O. A mixture of $^iPr_2NH$ (10 mL)/THF (20 mL)/CH_3CN (50 mL) was used to dissolve 4.06 × 10^{-5}−5.62 × 10^{-5} mol **5x** (**x** = **a**−**g**), 10 mol % of $Pd(PPh_3)_2Cl_2$, and 20 mol % of CuI. The mixture was stirred at rt for 15 min before addition of 1.2 equiv of [Os(4′-ethynylterpy)(terpy)]$(PF_6)_2$ **6**. After refluxing for about 24 h, the red-brown mixture was stripped of all solvent. The residue was redissolved in CH_3NO_2 and filtered. The CH_3NO_2 filtrate was washed with dilute HCl, Na_2CO_3 (aq), and water and dried over $MgSO_4$. The crude product was purified by silica column chromatography using CH_3CN/H_2O/saturated KNO_3 (85/14/1) as the eluent. The combined fractions containing the desired product were reduced in volume, and a KPF_6 aqueous solution was added to precipitate the product. The red-brown solid was collected, and washed with H_2O under centrifugation. Pure product was obtained by multiple recrystallization from CH_3CN/ether.

RC1O: 60 mg (4.98 × 10^{-5} mol) of **5a**; yield 40 mg (39%); ^{1}H NMR (δ, 500 MHz, CD_3CN) 5.82 (s, 2H), 7.04−7.26 (m, 8H), 7.29−7.31 (m, 4H), 7.41−7.45 (m, 4H), 7.64 (d, J = 1.8 Hz, 1H), 7.66 (d, J = 1.8 Hz, 1H), 7.73 (dd, J = 8.2 Hz, J = 1.8 Hz, 1H), 7.75 (dd, J = 8.2 Hz, J = 1.8 Hz, 1H), 7.81−7.89 (m, 4H), 7.96−8.04 (m, 5H), 8.07 (d, J = 8.2 Hz, 2H), 8.48 (t, J = 8.1 Hz, 1H), 8.51−8.58 (m, 8H), 8.80−8.83 (m, 4H), 8.943 (s, 2H), 8.950 (s, 2H); MALDI-MS (matrix: DCTB) (*m*/*z*) 1903.3 (calcd 1903.2 for $[M - PF_6]^+$), 1756.4 (calcd 1756.5 for $[M - 2PF_6]^+$), 878.2 (calcd 878.3 for $[M - 2PF_6]^{2+}$). Anal. Calcd for $RuOsC_{77}H_{50}N_{12}O_2 \cdot P_4F_{24} \cdot 3H_2O$: C, 44.03; H, 2.69; N, 8.00. Found: C, 44.00; H, 2.33; N, 8.16.

RC2O: 60 mg (4.93 × 10^{-5} mol) of **5b**; yield 35 mg (34%); ^{1}H NMR (δ, 500 MHz, CD_3CN) 4.25 (d, br, 2H), 4.67 (d, br, 2H), 7.14−7.26 (m, 8H), 7.30−7.31 (m, 4H), 7.41−7.45 (m, 4H), 7.65−7.74 (m, 6H), 7.81−7.87 (m, 4H), 7.96−8.02 (m, 5H), 8.48 (t, J = 8.3 Hz, 1H), 8.51−8.58 (m, 8H), 8.80−8.83 (m, 4H), 8.938 (s, 2H), 8.945 (s, 2H); MALDI-MS (matrix: DCTB) (*m*/*z*) 1915.2 (calcd 1915.2 for $[M - PF_6]^+$), 1770.3 (calcd 1770.6 for $[M - 2PF_6]^+$), 886.6 (calcd 885.3 for $[M - 2PF_6]^{2+}$). Anal. Calcd for $RuOsC_{78}H_{52}N_{12}O_2 \cdot P_4F_{24} \cdot 3H_2O$: C, 44.30; H, 2.76; N, 7.95. Found: C, 44.13; H, 2.55; N, 7.92.

RC3O: 60 mg (4.06 × 10^{-5} mol) of **5c**; yield 34 mg (41%); ^{1}H NMR (δ, 500 MHz, CD_3CN) 2.1 (buried under H_2O signal, 2H), 4.58 (t, br, 4H), 7.13−7.26 (m, 8H), 7.30−7.31 (m, 4H), 7.41−7.45 (m, 4H), 7.54−7.67 (m, 6H), 7.82−7.88 (m, 4H), 7.96−8.02 (m, 5H), 8.48 (t, J = 8.1 Hz, 1H), 8.51−8.58 (m, 8H), 8.80−8.83 (m, 4H), 8.929 (s, 2H), 8.934 (s, 2H); ESI-MS (*m*/*z*) 892.2 (calcd 892.1 for $[M - 2PF_6]^{2+}$), 746.4 (calcd 747.3 for $[M - 4PF_6]^{2+}$), 547.1 (calcd 546.5 for $[M - 3PF_6]^{3+}$), 373.9 (calcd 373.8 for [M

$- 4PF_6]^{4+}$). Anal. Calcd for $RuOsC_{79}H_{54}N_{12}O_2 \cdot P_4F_{24} \cdot 2H_2O$: C, 44.96; H, 2.77; N, 7.96. Found: C, 44.90; H, 2.84; N, 7.95.

RC4O: 70 mg (5.62×10^{-5} mol) of **5d**; yield 31 mg (26%); ^{1}H NMR (δ, 500 MHz, CD_3CN) 1.9 (buried under CD_3CN signal, 4H), 4.40 (t, br, 2H), 4.70 (m, br, 2H), 7.13−7.26 (m, 8H), 7.30−7.31 (m, 4H), 7.41−7.45 (m, 4H), 7.54−7.61 (m, 6H), 7.82−7.88 (m, 4H), 7.96−8.03 (m, 5H), 8.48 (t, $J = 8.3$ Hz, 1H), 8.51−8.58 (m, 8H), 8.80−8.83 (m, 4H), 8.935 (s, 2H), 8.939 (s, 2H); MALDI-TOF (matrix: DCTB) (*m*/*z*) 1945.3 (calcd 1945.2 for $[M - PF_6]^+$), 1800.3 (calcd 1798.6 for $[M - 2PF_6]^+$), 899.1 (calcd 899.3 for $[M - 2PF_6]^{2+}$). Anal. Calcd for $RuOsC_{79}H_{54}N_{12}O_2 \cdot P_4F_{24} \cdot 3H_2O$: C, 44.85; H, 2.92; N, 7.84. Found: C, 44.74; H, 2.97; N, 7.87.

RCE4O: 57 mg (9.3×10^{-6} mol) of **5e**; yield 35 mg (37%); ^{1}H NMR (δ, 500 MHz, CD_3CN) 3.54 (s, 4H), 3.73−3.74 (m, 4H), 3.97−4.01 (m, 2H), 4.37−4.42 (m, 2H), 7.09−7.24 (m, 8H), 7.26 (m, 4H), 7.36−7.42 (m, 10H), 7.78−7.81 (m, 4H), 7.92−7.97 (m, 5H), 8.46 (t, $J = 8.1$ Hz, 1H), 8.48−8.52 (m, 8H), 8.75−8.78 (m, 4H), 8.87 (s, 2H), 8.88 (s, 2H); MALDI-TOF (matrix: DCTB) (*m*/*z*) 2005.2 (calcd 2005.2 for $[M - PF_6]^+$).

RCE5O: 60 mg (4.44×10^{-5} mol) of **5f**; yield 40 mg (42%); ^{1}H NMR (δ, 500 MHz, CD_3CN) 3.63−3.71 (m, 8H), 3.84−3.92 (m, 4H), 4.20−4.24 (m, 2H), 4.41−4.46 (m, 2H), 7.14−7.26 (m, 8H), 7.30 (m, 4H), 7.41−7.54 (m, 10H), 7.82−7.88 (m, 4H), 7.96−8.02 (m, 5H), 8.48 (t, $J = 8.3$ Hz, 1H), 8.51−8.58 (m, 8H), 8.80−8.83 (m, 4H), 8.936 (s, 2H), 8.940 (s, 2H); MALDI-TOF (matrix: DCTB) (*m*/*z*) 2048.9 (calcd 2049.3 for $[M - PF_6]^+$), 1903.0 (calcd 1902.7 for $[M - 2PF_6]^+$), 952.0 (calcd 951.4 for $[M - 2PF_6]^{2+}$). Anal. Calcd for $RuOsC_{84}H_{64}N_{12}O_5 \cdot P_4F_{24} \cdot 2H_2O$: C, 45.27; H, 3.08; N, 7.54. Found: C, 45.09; H, 3.02; N, 7.67.

RCE6O: 60 mg (4.30×10^{-5} mol) of **5g**; yield 25 mg (26%); ^{1}H NMR (δ, 500 MHz, CD_3CN) 3.58−3.68 (m, 12H), 3.83−3.85 (m, 4H), 4.27−4.30 (m, 2H), 4.40−4.44 (m, 2H), 7.13−7.26 (m, 9H), 7.30−7.31 (m, 4H, 7.41−7.57 (m, 9H), 7.81−7.87 (m, 4H), 7.96−8.02 (m, 5H), 8.48 (t, $J = 8.3$ Hz, 1H), 8.51−8.58 (m, 8H), 8.80−8.83 (m, 4H), 8.927 (s, 2H), 8.932 (s, 2H); MALDI-TOF (matrix: DCTB) (*m*/*z*) 2093.4 (calcd 2093.3 for $[M - PF_6]^+$), 1946.4 (calcd 1946.8 for $[M - 2PF_6]^+$), 972.7 (calcd 973.4 for $[M - 2PF_6]^{2+}$). Anal. Calcd for $RuOsC_{86}H_{68}N_{12}O_6 \cdot P_4F_{24} \cdot 2H_2O$: C, 45.45; H, 3.19; N, 7.40. Found: C, 45.34; H, 3.11; N, 7.51.

Acknowledgment. This work was supported by the EPSRC (GR/R23305) and the University of Newcastle. We thank the EPSRC-sponsored Mass Spectrometry Service at Swansea and the University of Sheffield for collecting electrospray and MALDI mass spectra. Dr. P. Ghi is also thanked for help with obtaining low-temperature NMR spectra, Dr. R. W. Harrington for X-ray analysis, and Johnson Matthey for the loan of precious metals salts.

Supporting Information Available: General experimental procedures. ^{1}H NMR spectra for all new compounds, as well data for the X-ray crystal structure of **RC1**, electrospray mass spectrometry results, and results from the computational studies. This material is available free of charge via the Internet at http://pubs.acs.org.

JO0600555